

4-2022

POSSIBLE STORAGE OF CO₂ IN SALINE AQUIFER: STORAGE FACTOR ESTIMATION

Sarah Abdul Aziz Al-Tamimi

Follow this and additional works at: https://scholarworks.uaeu.ac.ae/all_theses



Part of the [Petroleum Engineering Commons](#)

Recommended Citation

Al-Tamimi, Sarah Abdul Aziz, "POSSIBLE STORAGE OF CO₂ IN SALINE AQUIFER: STORAGE FACTOR ESTIMATION" (2022). *Theses*. 894.

https://scholarworks.uaeu.ac.ae/all_theses/894

This Thesis is brought to you for free and open access by the Electronic Theses and Dissertations at Scholarworks@UAEU. It has been accepted for inclusion in Theses by an authorized administrator of Scholarworks@UAEU. For more information, please contact mariam_aljaberi@uaeu.ac.ae.



MASTER THESIS NO. 2022:11

College of Engineering

Department of Chemical and Petroleum Engineering

**POSSIBLE STORAGE OF CO₂ IN SALINE AQUIFER:
STORAGE FACTOR ESTIMATION**

Sarah AbdulAziz Al-Tamimi



April 2022

United Arab Emirates University
College of Engineering
Department of Chemical and Petroleum Engineering

POSSIBLE STORAGE OF CO₂ IN SALINE AQUIFER: STORAGE FACTOR
ESTIMATION

Sarah AbdulAziz Al-Tamimi

This thesis is submitted in partial fulfillment of the requirements for the degree of Master of
Science in Petroleum Engineering

Under the Supervision of Professor Abdulrazag Y. Zekri

April 2022

Declaration of Original Work

I, Sarah AbdulAziz Al-Tamimi, the undersigned, a graduate student at the United Arab Emirates University (UAEU), and the author of this thesis entitled “*Possible Storage of CO₂ in Saline Aquifer: Storage Factor Estimation*”, hereby, solemnly declare that this thesis is my own original research work that has been done and prepared by me under the supervision of Prof. Abdulrazag Y. Zekri, in the College of Engineering at UAEU. This work has not previously formed the basis for the award of any academic degree, diploma or a similar title at this or any other university. Any materials borrowed from other sources (whether published or unpublished) and relied upon or included in my thesis have been properly cited and acknowledged in accordance with appropriate academic conventions. I further declare that there is no potential conflict of interest with respect to the research, data collection, authorship, presentation and/or publication of this thesis.

Student's Signature: *Sarah Al-Tamimi* Date: 25/05/2022

Copyright© 2022 Sarah AbdulAziz Al-Tamimi
All Rights Reserved

Advisory Committee

1) Advisor: Prof. Abdulrazag Y. Zekri

Title: Professor

Department: Chemical and Petroleum Engineering

College of Engineering

2) Member: Dr. Gamal Alusta

Title: Associate Professor

Department: Chemical and Petroleum Engineering

College of Engineering

3) Member (External Examiner): Prof. Eric Mackay

Title: Professor of Energy, Geoscience, Infrastructure and Society

Department: GeoEnergy Engineering

College: Heriot Watt University, United Kingdom

Approval of the Master Thesis

This Master Thesis is approved by the following Examining Committee Members:

1) Advisor (Committee Chair): Prof. Abdulrazag Y. Zekri

Title: Professor

Department: Chemical and Petroleum Engineering

Signature _____  Date 4/26/2022

2) Member: Dr. Gamal Alusta

Title: Associate Professor

Department: Chemical and Petroleum Engineering

Signature _____  Date 4/28/2022

3) Member (External Examiner): Prof. Eric Mackay

Title: Professor of Energy, Geoscience, Infrastructure and Society

Department: GeoEnergy Engineering

College: Heriot Watt University, United Kingdom

Signature _____  Date 4/28/2022 _____

This Master Thesis is accepted by:

Acting Dean of the College of Engineering: Professor Mohamed Al-Marzouqi

Signature Mohamed AlMarzouqi Date June 07, 2022

Dean of the College of Graduate Studies: Professor Ali Al-Marzouqi

Signature Ali Hassan Date June 07, 2022

Abstract

The objective of this study is to perform laboratory measurements and CO₂ underground storage study to cover the knowledge gap on CO₂-Brine relative permeability and assess various variables on the storage of CO₂ in a selected aquifer. Several factors that affect CO₂ storage have been discussed in the literature. These include both macroscopic and microscopic displacement efficiency of brine as a function of CO₂ pore volume injected. It is clear from the literature that there is still more work needed to investigate the effect of various variable such as formation temperature, brine viscosity, and possible presence of free gas in the aquifer on the CO₂ storage efficiency of the selected aquifer.

Experimental tests were conducted on four carbonate-limestone core samples to determine the capillary pressure curves and to conduct CO₂ flooding into 100% brine saturated core samples. Each core sample has with different brine salinity. Flooding tests were conducted at constant injection pressure yet, the injection temperature for each core sample was different. Brooks-Corey correlation was used to obtain the relative permeability curves of CO₂ -Brine system. Using experimental results of capillary pressure, modified Ritter and Drake correlation was used to determine the pore throat size distribution.

This thesis research shows the results of limestone core flooding tests and CO₂ flooding of an aquifer runs obtained using Petroleum Solution software to evaluate the effect of brine viscosity, temperature, gas saturation on aquifer CO₂ storage capacity (storage factor). The results revealed that the CO₂ storage capacity increases as temperature increase because of thermal effects. Whereas, as the gas saturation increases, the storage capacity of the selected zone decreases. In addition to that, the flooding runs showed that relatively high viscosity brine aquifer hider the CO₂ storage capacity of the reservoir.

Keywords: Relative Permeability, Enhanced Oil Recovery, CO₂ Flooding, Capillary Pressure, CO₂ Storage Factor, Brine Saturation, Brine Salinity, Irreducible Water Saturation (Swirr), Drainage Displacement, Wettability.

Title and Abstract (in Arabic)

التخزين المحتمل لثاني أكسيد الكربون في طبقة المياه المالحة: تقدير معامل التخزين

الملخص

الهدف من هذه الدراسة هو إجراء القياسات المختبرية ودراسة التخزين تحت الأرض لثاني أكسيد الكربون لتغطية الفجوة المعرفية حول النفاذية النسبية لثاني أكسيد الكربون ومحلل ملح وتقييم المتغيرات المختلفة على تخزين ثاني أكسيد الكربون في طبقة المياه الجوفية المختارة. تمت مناقشة العديد من العوامل التي تؤثر على تخزين ثاني أكسيد الكربون في الأدبيات. وهي تشمل كلاً من كفاءة الإزاحة المجهريّة والميكروسكوبية للمحلل الملح كدالة لحجم مسام ثاني أكسيد الكربون المحقون. يتضح من الأدبيات أنه لا يزال هناك المزيد من العمل المطلوب لاستقصاء تأثير المتغيرات المختلفة مثل درجة حرارة التكوين، ولزوجة المحلول الملحي، واحتمال وجود غاز حر في الخزان الجوفي على كفاءة تخزين ثاني أكسيد الكربون في الخزان الجوفي المحدد.

أجريت اختبارات تجريبية على أربع عينات أساسية من الحجر الجيري الكربوني لتحديد منحنيات الضغط الشعري ولإجراء غمر ثاني أكسيد الكربون في عينات القلب المشبعة بالمحلل الملح بنسبة 100%. كل عينة أساسية لديها ملوحة ملحية مختلفة. أجريت اختبارات الغمر عند ضغط حقن ثابت، لكن درجة حرارة الحقن لكل عينة لينة كانت مختلفة. تم استخدام ارتباط Brooks-Corey للحصول على منحنيات النفاذية النسبية لنظام ثاني أكسيد الكربون- محلل ملح. باستخدام النتائج التجريبية للضغط الشعري، تم استخدام ارتباط ريتز ودريك المعدل لتحديد توزيع حجم الحلق المسامي.

يمثل هذا البحث نتائج اختبارات الغمر الأساسية للحجر الجيري وفيضان ثاني أكسيد الكربون لطبقات المياه الجوفية التي تم الحصول عليها باستخدام برنامج بتروليوم لتقييم تأثير لزوجة المحلول الملحي ودرجة الحرارة وتشبع الغاز على سعة تخزين طبقة المياه الجوفية (عامل التخزين). أوضحت النتائج أن السعة التخزينية لثاني أكسيد الكربون تزداد مع زيادة درجة الحرارة بسبب التأثيرات الحرارية. حيث إنه مع زيادة تشبع الغاز، تقل سعة التخزين للمنطقة المحددة. بالإضافة إلى ذلك، أظهرت مسارات الغمر أن طبقة المياه المالحة ذات اللزوجة العالية نسبياً تخفي سعة تخزين ثاني أكسيد الكربون في الخزان.

مفاهيم البحث الرئيسية: النفاذية النسبية، الاستخلاص المعزز للنفط، غمر ثاني أكسيد الكربون، الضغط الشعري، عامل تخزين ثاني أكسيد الكربون، تشبع المحلول الملحي، ملوحة المحلول الملحي، تشبع نزوح الصرف، قابلية التبلل المياه غير القابل للاختزال.

Acknowledgments

First and foremost, praise and thanks to God, the Almighty, for His blessings throughout my research work to complete the research successfully.

I would like to express my deep and sincere gratitude and appreciation to my research supervisors, Prof. Abdulrazag Y. Zekri and Dr. Gamal Alusta for their continuous support of my research, for their enthusiasm, motivation, patience, and immense knowledge. Their support and guidance helped me through this thesis, it was a great honor and privilege working under their guidance. I could not have imagined having a better supervisor.

I am extremely grateful to my family for their constant love, care, prayers, support, and sacrifices for educating me. Special thanks to my mother, Dr. Wejdan Abdul Razzaq Mansoor, I want to express my deepest gratitude for your continuous support, inspiration, and guidance throughout the completion of my master's degree and research. Your help and encouragement are appreciated.

Last but not the least, I would like to thank Lab Engineer Essa for his great efforts and help during the experiment work. He taught me and guide me during the experimental work. I gained a lot of knowledge related to lab experiments and how to handle the equipment. In addition, I learned from him how to be patient and other life philosophies.

Dedication

To my beloved parents and family

Table of Contents

Title.....	i
Declaration of Original Work.....	ii
Copyright.....	iii
Advisory Committee.....	iv
Approval of the Master Thesis	v
Abstract.....	vii
Title and Abstract (in Arabic).....	viii
Acknowledgments	ix
Dedication.....	x
Table of Contents.....	xi
List of Tables	xiii
List of Figures.....	xiv
List of Abbreviations	xvi
Chapter 1: Introduction.....	1
1.1 Overview.....	1
1.2 Problem Statement.....	2
Chapter 2: Literature Review	4
2.1 EOR Applications / Recovery Mechanisms	4
2.2 Carbon dioxide (CO ₂)-EOR Techniques	5
2.3 CO ₂ Displacement.....	8
2.3.1 Macroscopic Displacement.....	8
2.3.2 Microscopic Displacement.....	17
2.4 CO ₂ Supercritical	18
Chapter 3: Methodology.....	21
3.1 Core Cut Machine.....	21
3.2 Cleaning Samples (Stark and Dean Method).....	21
3.3 Core Dimensions.....	22
3.4 Liquid Permeability and Porosity Measurements.....	22
3.4 Brines Preparation.....	23
3.5 Vacuum and Pressure Method Saturation.....	24
3.6 Porous Plate Technique.....	25
3.7 Carbon Dioxide Flooding	26
Chapter 4: Experimental Results	27
4.1 Capillary Pressure	27
4.2 Relative Permeability.....	32
4.3 CO ₂ Storage Factor	37
Chapter 5: Discussion.....	49
5.1 Capillary Pressure and Pore Size Distribution.....	49

5.2 CO ₂ Flooding Analysis	50
5.3 CO ₂ Storage Factor	51
Chapter 6: Conclusions and Recommendations	53
6.1 Summary	53
6.2 Conclusion	53
6.3 Recommendations.....	53
References.....	54
Appendices	56
Appendix A.....	56
Appendix B	58
Appendix C	60

List of Tables

Table 1: Core sample dimensions	22
Table 2: Rock properties of core samples	23
Table 3: Brine salinity for each core sample.....	24
Table 4: CO ₂ flooding conditions	26
Table 5: Residual CO ₂ saturation obtained during CO ₂ flooding test.....	33
Table 6: Irreducible water saturation obtained from porous plate experiment	49
Table 7: Pore throat size distribution results.....	50
Table 8: Capillary pressure results for core sample 9A	56
Table 9: Capillary pressure curve for core sample 12A.....	56
Table 10: Capillary pressure curve for core sample 13A.....	57
Table 11: Capillary pressure curve for core sample 12A.....	57
Table 12: Pore throat size distribution results for core sample 9A	58
Table 13: Pore throat size distribution results for core sample 12A	58
Table 14: Pore throat size distribution results for core sample 13A	59
Table 15: Pore throat size distribution results for core sample 14A	59
Table 16: CO ₂ flooding test for sample 9A.....	60
Table 17: CO ₂ flooding test for sample 12A.....	61
Table 18: CO ₂ flooding test for sample 13A.....	61
Table 19: CO ₂ flooding test for sample 14A.....	62

List of Figures

Figure 1: Slim tube displacement to determine the MMP	7
Figure 2: Wetting angles for different wetting phases	10
Figure 3: Relative permeability curves for sandstone core sample	14
Figure 4: Capillary pressure curves for coquina sample	16
Figure 5: Imbibition relative permeability curves for coquina sample	17
Figure 6: Density of carbon dioxide in relation pressure and temperature	19
Figure 7: Experimental core samples	21
Figure 8: Brine mixing apparatus	24
Figure 9: Vacuum and pressure apparatus	25
Figure 10: Primary drainage capillary pressure curve at 50,000 ppm brine salinity	27
Figure 11: Primary drainage capillary pressure curve at 100,000 ppm brine salinity	28
Figure 12: Primary drainage capillary pressure curve at 200,000 ppm brine salinity	28
Figure 13: Primary drainage capillary pressure curve at 250,000 ppm brine salinity	29
Figure 14: Pore entry size distribution for core sample 9A	30
Figure 15: Pore entry size distribution for core sample 12A	31
Figure 16: Pore entry size distribution for core sample 13A	31
Figure 17: Pore entry size distribution for core sample 14A	32
Figure 18: Relative permeability curve for core sample 9A	34
Figure 19: Relative permeability curve for core sample 12A	35
Figure 20: Relative permeability curve for core sample 13A	35
Figure 21: Relative permeability curve for sample 14A	36
Figure 22: Production rate vs. cumulative time at 200°F	36
Figure 23: Production rate vs. cumulative time at 300°F	37
Figure 24: Production rate vs. cumulative time at 350°F	37
Figure 25: CO ₂ storage factor versus pore volume injected for 200°F	39
Figure 26: CO ₂ storage factor versus pore volume injected for 300°F	39
Figure 27: CO ₂ storage factor versus pore volume injected for 350°F	40
Figure 28: Maximum CO ₂ storage factor at each temperature	40
Figure 29: CO ₂ storage factor at breakthrough at each temperature	41
Figure 30: CO ₂ storage factor versus pore volume of CO ₂ injected for S _{gi} = 2%	42
Figure 31: CO ₂ storage factor versus pore volume injected for S _{gi} = 5%	42
Figure 32: CO ₂ storage factor versus pore volume injected for S _{gi} = 8%	43
Figure 33: CO ₂ storage factor versus pore volume injected for S _{gi} = 10%	43

Figure 34: Maximum CO ₂ storage factor at each initial HC gas saturation	44
Figure 35: CO ₂ storage factor at breakthrough at each HC initial gas saturation	44
Figure 36: CO ₂ storage factor versus pore volume injected for 0.1 cp brine viscosity	45
Figure 37: CO ₂ storage factor versus pore volume injected for 0.15 cp brine viscosity	46
Figure 38: CO ₂ storage factor versus pore volume injected for 0.2 cp brine viscosity	46
Figure 39: CO ₂ storage factor versus pore volume injected for 0.25 cp brine viscosity	47
Figure 40: Maximum CO ₂ storage factor at each brine viscosity.....	47
Figure 41: CO ₂ storage factor at breakthrough at each brine viscosity.....	48

List of Abbreviations

CO ₂	Carbon Dioxide
Cum	Cumulative
EOR	Enhanced Oil Recovery
HC	Hydrocarbon
Inj.	Injection
Krco ₂	Carbon Dioxide Relative Permeability
OOIP	Original Oil In Place
P _c	Capillary pressure
Prod	Production
PV	Pore Volume
S _{gi}	Gas Saturation
Sw _{irr}	Irreducible Brine Saturation

Chapter 1: Introduction

1.1 Overview

Carbon dioxide (CO₂) injection is dominant among enhanced oil recovery methods to maintain oil production rate and reserves. This technique will continue to be applied in the industry to produce the trapped underground reserves. CO₂ is a naturally occurring source of gas that can be extracted in large quantities and injected into underground formations. Thus, CO₂ is relatively inexpensive.

Injecting Carbon dioxide (CO₂) into oil formations has the potential to recover around 15% to 20% of original oil into existing wells. Hence, knowledge of the geologic features, mainly rocks and fluid characteristics, can influence the oil and gas movement. Better understanding of porosity, permeability and reservoir structural features such as faults can lead to precise estimation of Original Oil In Place (OOIP). Selection of miscible CO₂ injection technique depends on the geological reservoir geology, oil gravity & viscosity as well as Minimum Miscibility Pressure (MMP). Basically, identification of how CO₂ reacts with trapped oil is required to determine the miscibility property of CO₂. Primarily, CO₂ at supercritical pressure and temperature will be completely miscible with oil (Verma, 2015).

Different CO₂ -EOR flooding recovery techniques are conducted depending on the reservoir geology, rock and fluid properties, production and injection well pattern as well as the time at which relative water-flooding is considered. Basically, the main two techniques are to displace trapped oil into production wells. The two techniques are: continuous CO₂ injection and Conventional Water Alternating Gas (WAG) followed with water. The first technique is considered as primary recovery at which CO₂ is continuously injected into the reservoir without any fluid pumped afterwards. This technique is suitable for medium to light oil reservoirs as well as strongly water-wet reservoirs which are water-sensitive to water-flooding. Whereas, Water Alternating Gas (WAG) technique is conducted by injecting the volume of CO₂ in cycles,

followed by equal volumes of water. The injected water aids in improving the CO₂ sweeping efficiency, leading to a reduction in CO₂ channeling across the reservoir (Verma, 2015).

Several researchers provided technical information related to CO₂-EOR method describing the relative permeability of fluids in CO₂/Oil system. Although, over the last decade, not much data covering the CO₂-Brine relative permeability can be found in the published literature. Therefore, it is evident that more experiments are needed to cover this knowledge gap on CO₂-Brine relative permeability. This proposed experimental work will be performed employing unsteady state experimental approach, and investigate different experimental parameters such as temperature, pressure, brine concentration and composition, pore size distribution, and injection rate effect on the measurements of CO₂-Brine relative permeability. established to determine initial brine and residual CO₂ saturations, as well as relative permeability of the flow system. In addition, several factors were included, such as flow distribution across the reservoir and phase composition of CO₂/Brine system (Verma, 2015).

1.2 Problem Statement

Oil reservoirs follow a series of production stage with time. The first stage highly depends on the natural differential pressure between surface and underground well. This stage is called primary technique. Basically, in primary stage the reservoir produces naturally without any at intervention. Over time, due to a decline in oil production, efficient techniques are implemented to recover trapped oil in the reservoir. Those alternative methods are implemented, such as Enhanced Oil Recovery (EOR) techniques which can provide around 30 to 60 % or even more of the reservoir's original oil in place. Commercial EOR methods are implemented in the oil and gas industry to extract more oil, which highly depends on the reservoir characteristics as well as the long-term field life of mature hydrocarbon resources (Andrei et al., 2010).

CO₂ injection into underground formations has been practiced for several years in the oil and gas industry. This is because using CO₂ injection as Enhanced Oil Recovery (EOR) technique to enhance oil recovery factor at the final phase of the reservoir life and thus extend the production

life. Injecting CO₂ in supercritical phase can flow through the porous and permeable zones and thus releasing the trapped oil into the producer well. Moreover, fraction of the injected CO₂ will be stored underground which has direct environment benefit (Andrei et al., 2010).

Although CO₂ has been employed in enhanced oil recovery, not much data covering the CO₂-Brine relative permeability can be found in the published literature. The limited studies available reported broad ranges for CO₂ relative permeability in typical sedimentary rocks, such as Berea sandstone, dolomite, and others. No detailed experimental data covering limestone rocks are available for researchers. Therefore, it is evident that more experiments are needed to cover this knowledge gap on CO₂-Brine relative permeability. This proposed experimental work provide unsteady state experimental approach to investigate the capillary pressure, relative permeability as well as wettability indication of CO₂/Brine system.

Chapter 2: Literature Review

2.1 EOR Applications / Recovery Mechanisms

Production of hydrocarbons is typically implemented in two or three economically feasible phases: primary, secondary and tertiary recovery. Initial recovery from oil-bearing formation is accomplished by nature reservoir energy. The main sources of natural reservoir energy that lead to primary production include the difference in reservoir pressure and bottom-hole pressure, which forces the oil to flow from the reservoir into the well then, to the surface. In addition, communicating nearby water aquifers and gravity drainage could help to displace the hydrocarbons with natural energy. The primary recovery classification could also include gas lift and pumping to maintain the production when the reservoir energy has been depleted. The recovery factor of the primary recovery is around an average of 5-25% of OOIP (Original Oil In Place). This typical range can vary based on the geological characteristics of the reservoir and reservoir pressure (Andrei et al., 2010).

EOR techniques have been lumped into categories: secondary and tertiary recovery techniques. As the primary recovery techniques are no longer feasible and effective, those techniques provide additional energy to produce hydrocarbons from reservoirs. Secondary recovery is the attempt to supply energy from an external source to maintain or increase the reservoir pressure. Typical techniques used in the industry are water flooding, or natural gas referred to as gas flooding. The use of this technique is to inject into the reservoir re-pressurize the reservoir pressure and maintain it at high pressure. The recovery factor of this technique depends on the oil and reservoir characteristics. The typical range of recovery factors is between 6-30% of OOIP (Original Oil In Place) (Andrei et al., 2010).

The purpose of the tertiary recovery is to displace the residual oil saturation left behind that cannot be displaced or produced through secondary techniques. Enhanced Oil Recovery (EOR) applications are conducted in oilfields approaching the end of their life. Tertiary recovery

techniques can be classified as miscible flooding, chemical flooding, and thermal flooding. Miscible flooding technique involves injecting fluids that are miscible with the reservoir hydrocarbons, such as carbon dioxide injection under miscible conditions. The gas will mix with the reservoir oil to lower the viscosity of the oil. This technique will allow the oil to be displaced from the reservoir. Chemical flooding includes the injection of polymers into the reservoir. Polymers and additional chemicals to the injected water will generate a combination of phase behavior change and reduction of Interfacial Tension (IFT) or increasing solution water viscosity. This technique is unfeasible in the industry due to the high cost of the chemicals and limitations of temperature. Typically, miscible and chemical flooding are implemented in reservoirs that contain light crude oil (15-30 API). Whereas, injection of hot water and steam cycling are methods categorized as thermal flooding. Oil viscosity is reduced as additional heat is injected into the reservoir to allow oil to be displaced. In reservoirs that contain heavy crude oil (> 30 API), thermal flooding is considered to be used. Also, the range of tertiary recovery factors differs based on the type of crude oil. In light crude oil, the range is between 5-15% of OOIP (Original Oil In Place) and lower in heavy crude oils (Andrei et al., 2010).

2.2 Carbon dioxide (CO₂)-EOR Techniques

The carbon dioxide (EOR-CO₂) technique is used to extend the field's productive life and to increase oil production at the end lift of the reservoir. In addition to that, this technique is the most feasible and attractive technique in the market. This is because CO₂ can be captured inexpensively at the point of combustion in order to mitigate the emission of CO₂. Then, the CO₂ is stored in underground reservoirs to reduce the CO₂ atmospheric emissions.

Carbon dioxide is injected into the oil reservoir passing through the void spaces where no water is invaded previously, to displace the trapped oil. As CO₂ is injected into the reservoir, some remaining CO₂ will be stored underground, this is considered beneficial to the environment. There are two practical methods to inject CO₂ into the oil reservoir depending on the reservoir oil

characteristics as well as reservoir pressure and temperature. The two methods are miscible and immiscible displacement (El-hoshoudy & Desouky, 2018).

Miscible displacement employs by injecting CO₂ into an oil reservoir at the supercritical phase to displace the trapped oil reservoir. CO₂ will improve the oil recovering by dissolving and becoming mutual soluble with the trapped reservoir oil as light hydrocarbons from the reservoir oil will be dissolved. This technique will decrease the interfacial tension between the two fluids forming a reduction in the viscosity to displace and produce the oil easily. CO₂ is injected and dissolved completely at Minimum Miscibility Pressure (MMP). The Minimum Miscibility Pressure (MMP) is defined as the lowest pressure at which the injected CO₂ and trapped oil become miscible at constant reservoir temperature and composition. At the MMP, the interfacial tension is almost zero and an interface exists between the fluids. In cases where the reservoir pressure is above the MPP, the miscibility can be achieved through multiple-contact or dynamic miscibility. In this case, the condensed gas-drive process is achieved to allow two phases to become miscible without an interface (El-hoshoudy & Desouky, 2018). This method comprises of three contacts:

- First contact: inject miscible solvent to mix with reservoir oil to be in one phase.
- Vaporizing gas-drive process: inject lean gases or CO₂ where intermediate and high molecular weight hydrocarbons from the reservoir oil to achieve miscibility by in situ vaporization.
- Condensing gas-drive process: this stage is achieved through a condensation process in which in situ intermediate molecular weight hydrocarbons in the solvent are transferred into the lean reservoir oil.

In the industry, Slimtube is one of the most common test methods conducted in conditions where the miscible displacement. The purpose of the slim tube is to measure the MMP. The slim tube test is conducted by injecting the CO₂ into a fully oil-saturated slim tube at different pressures

and rates. As the volume of injected CO₂, pressure, and the rate is known, the oil recovery is obtained during the experiment. Figure 1 shows the oil recovery at a 1.2 pore volume of CO₂ injected at each pressure. The recovery increases up to 98% at CO₂ breakthrough as the pressure increases. At some point the pressure starts to be stable, this point can be identified as the Minimum Miscibility Pressure (MMP). In other words, it is the pressure at which it starts to deviate and the achieved maximum recovery is set constant. Above the MMP, the displacement is called multiple contact or dynamic miscible displacement which means the CO₂ solvent is no longer miscible with the oil (PetroWiki, 2015).

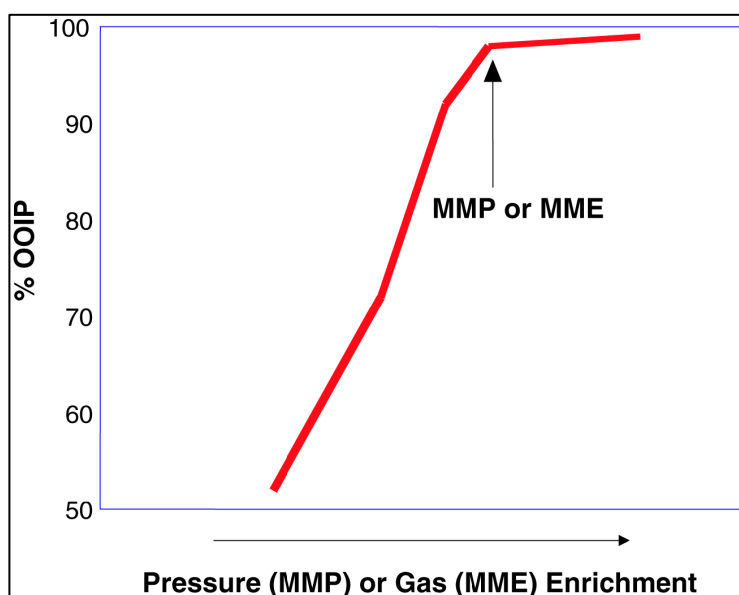


Figure 1: Slim tube displacement to determine the MMP

Immiscible displacement is referred to as immiscible flooding where injected gasses are not completely mixed with the reservoir oil. Immiscible CO₂ injection is conducted when the reservoir pressure is below the MMP or the density of the oil is too high. Meanwhile, CO₂ injection can cause the reservoir oil to swell by extracting the lighter components from the oil, which will reduce the density of the oil. Consequently, the recovery factor can be increased by

displacing the oil can be displaced and improving the mobility of the oil phase (El-hoshoudy & Desouky, 2018).

Most EOR projects focus on miscible flooding, although immiscible flooding could be more efficient. Concerns related to miscible flooding include asphaltene precipitation in the reservoir or in the piping system. This can occur if an adequate amount of volume is dissolved into the oil. Asphaltene precipitation can cause reservoir plugging where the pore throat can be plugged, as well as reducing the flow rate of the wells. This can reduce the oil recovery (NETL, 2010).

2.3 CO₂ Displacement

The displacement process of any fluid includes the macroscopic (volumetric displacement) and microscopic efficiencies. The overall recovery efficiency is the product of the microscopic and macroscopic efficiencies (Terry & Rogers, 2014; Equation 1).

$$E = E_v \times E_d \quad (1)$$

Macroscopic displacement measures how efficiently the displacing fluid has approached the oil-bearing zone in the reservoir. The microscopic displacement evaluates the efficiency of the displacing fluid in mobilizing the trapped oil (Terry & Rogers, 2014).

2.3.1 Macroscopic Displacement

The main factors that could affect the macroscopic displacement efficiency are interfacial tension, wettability, capillary pressure, and relative permeability (Terry & Rogers, 2014).

2.3.1.1 Interfacial Tension

The interfacial tension is the force of attractions that create an interface at the boundary between two fluids or rock-fluid. This occurs when a molecule near the interface has relatively different molecular interactions than the molecules in the bulk fluid. Different chemical agents

are used to reduce the interfacial tension, such as surfactants. The typical interfacial tension of oil-brine systems is between 20 to 30 dynes/cm (Terry & Rogers, 2014).

2.3.1.2 Wettability

Wettability is the tendency of a fluid to spread on a solid over another. The solid surface can be oil-wet or water-wet based on the chemical composition of the fluid and the rock. When the rock is water-wet, the water is in contact with the solid and the oil is the surrounding phase. Whereas, the oil-wet is when the oil is in contact with the rock surface. Wettability includes the measurement of contact angle to determine the degree of wetting between solid and liquid interaction. Contact angle or the wetting angle can be defined as the angle between the surface of the liquid and the outline of the contact surface. This angle is the angle that the liquid creates with a solid surface as in contact when occupied in small porous media. The wetting fluid is the one that preferentially spreads around the solid surface. Whereas, the other fluid is called the non-wetting fluid (Terry & Rogers, 2014). In a reservoir rock, the rock is preferentially water-wet if water wets the rock surface. Then, water is in the wetting phase when the contact angle is above 90 degrees. As the contact angle decreases below 90 degrees, the more the reservoir rock is considered to be strongly water-wet. If the spreading fluid is oil, the rock is preferentially oil-wet. In this case, the contact angle is above 90 degrees. Moreover, when the contact angle is equal to 90 degrees, the reservoir rock is considered to be neutral-wet when both fluids tend to wet the rock surface (Glover, 2015).

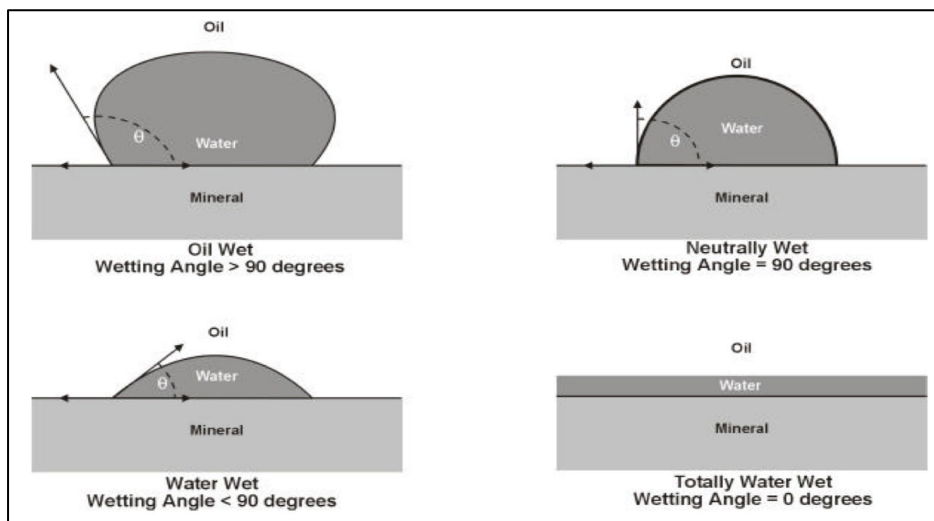


Figure 2: Wetting angles for different wetting phases

Wettability alteration is an important factor that needs to be approached in Enhanced Oil Recovery techniques (EOR). In most oil reservoirs, the rock is more to be water-wet before oil migrate. Hence, several factors can change the wetting state of the rock. The main factors include the composition of oil, water, and rock as well as the reservoir pressure and temperature can affect the wettability. Moreover, wettability has a great influence on the relative permeability, capillary pressure, and residual saturations. Oil displacement by CO_2 injection can trigger the wettability in which the CO_2 front or oil bank can move the water in contact with the rock surface if mobile leaving behind residual oil. Also, injected CO_2 can alter the equilibrium condition of the reservoir hydrocarbons which can cause asphaltene precipitation. The precipitation can alter the wettability and affect oil recovery. Asphaltene precipitation near the wellbore can decrease the productivity of the well. therefore, any change in oil composition can change the wettability from natural water-wet to oil-wet because the components of the oil phase are changing. The temperature, pressure, and composition of crude oil can disturb the stability of asphaltene (Abdallah et al., 2007).

2.3.1.3 Relative Permeability

Permeability is a measure of the ability of the fluid to flow through a porous rock for a specified pressure drop. Thus, permeability describes a rock property and it is independent of fluid type. This indicates permeability is highly dependent on the geometry of the pore network. Based on Darcy's law, an empirical Equation that describes a laminar flow of incompressible fluids relates the flow rate of a fluid with known viscosity to a pressure gradient that is proportional to permeability. Therefore, permeability is applied only to flow when the pores of the rock are saturated 100% of a single fluid. The permeability of a single fluid is called absolute permeability. Usually, permeability is typically expressed in Darcy (D) or milli-darcy (mD). Equation 2 shows a steady-state flow Equation in which absolute permeability can be calculated (Honarpour et al., 1992).

$$q = \frac{KA \Delta P}{\mu dL} \quad (2)$$

Where;

q: flow rate; bbls/day

k: permeability, mD

A: cross sectional area; ft²

In petroleum reservoirs, porous media are not fully saturated with a single-phase, different fluids may occupy the porous media such as gas, oil, and water. therefore, in a multiphase system, it is essential to measure the capability of each phase to flow through porous media in the presence of another phase. Thus, relative permeability is used to describe the concept of multiphase flow in the reservoirs. Relative permeability is defined as the ratio of the effective permeability of fluid to the absolute permeability of the rock. Effective permeability is a measure of the flow capability of that phase in the presence of other fluids. For example, the effective permeability of the oil

phase is to measure the flow capability of oil in the presence of water or both water and gas phases (Honarpour et al., 1992).

Relative permeability measurements are conducted in core samples in a laboratory to study the flow behavior of fluids in the reservoir. In a single-phase system, dry gas, or under-saturated oil reservoirs, the effective permeability of the mobile fluid that flows through the reservoir does not change. This is because the fluid saturation did not change. Hence, when more the fluid in the reservoir is mobile, the effective permeability will change in which the fluid saturation in the reservoir will change (Honarpour et al., 1992).

Laboratory experiments are conducted to gather relative permeability data to predict the productivity, injectivity, and ultimate recovery of the reservoirs to evaluate the reservoir and use it for simulation studies to plan further enhanced oil recovery techniques to improve the recovery of hydrocarbons from the reservoir. In addition, the data can be used to diagnose formation damage expected during production operation conditions (Honarpour et al., 1992).

As will be explained later, the objective of the laboratory experiment is to study the relative permeability of CO₂/Brine flow systems. Typically, researchers used two methods to measure the drainage and imbibition relative permeability under different flow, pressure, and temperature conditions. The two methods are steady and unsteady states. To experiment, a CT scanner is used to measure the saturation of in situ fluids. The porosity of the Sandstone core samples was measured using Boyle's law and X-ray imaging technique. Also, the absolute permeability of the brine was measured (Akbarabadi & Piri, 2013).

In the first category of the sandstone core samples, the unsteady-state method was conducted to measure the drainage and imbibition relative permeability. The experimental test was conducted at an ambient temperature and 3.46 MPa. The flow rate was increased gradually until the maximum value is reached. Before any test, the core samples were fully saturated with brine ($S_w = 1$). Basically, at the drainage process, the gaseous CO₂ was injected at maximum flow rate into the core samples till the maximum flow rate reached and obtained less than 1% in the

variation of pressure drop and saturation distribution across the core sample. The brine saturation at this stage is reported at initial brine saturation for the imbibition brine injection process. Moreover, in the imbibition stage, the flow rate of the injected brine is gradually increased this reached the maximum flow rate which was 0.375 cm³/min in 0.025 cm³/min incremental. The residual gaseous CO₂ saturation of the core sample is scanned and reported (Akbarabadi & Piri, 2013).

In the second group of the core sample, the steady-state method was performed. In this experiment, the test was conducted on sandstone core samples at high pressure and temperature, 11 MPa and 55 degrees Celsius respectively. At this condition, the state of CO₂ will be supercritical. First, the drainage experiment was carried out followed by the brine floods. Typically, the viscosity and density of critical saturation of CO₂ are higher than the gaseous CO₂. Therefore, the maximum flow rate reached during the test was 20 cm³/min. At this stage, several cycles of drainage and imbibition flow experiments were performed to obtain the relative permeability curves at a different range of flow rates. Before any cycle, the core samples were fully saturated with brine at the initial condition ($S_w = 1$). In the drainage process, the CO₂ displaces the brine till CO₂ critical saturation (SC_{CO_2}) is reached. The saturation at each cycle differs, for example, at the end of the drainage process, CO₂ critical saturation (SC_{CO_2}) is equal to 0.475 which leads to 0.525 brine saturation for the imbibition process. For each cycle, the pressure drop crosses the core sample and the in situ fluid saturation is recorded after reaching steady-state (Akbarabadi & Piri, 2013).

The observations of unsteady-state at drainage process indicate that the CO₂ critical saturation (SC_{CO_2}) increases sharply at lower flow rates. However, at high flow rates, SC_{CO_2} gradually starts to stabilize. The reason behind this phenomenon is that it becomes harder for the brine to be displaced in smaller pores and fractures as the brine saturation decreases. Furthermore, in the steady-state experiment, the results of relative permeabilities for drainage and imbibition flow tests are shown in Figure 2 for a sandstone core sample at two separate experiments

performed. In each cycle of drainage and imbibition flow test, the different saturation level of initial water saturation was established. In the first cycle, the initial water saturation is equal to 1. Hence, in the second cycle, the initial water saturation is approximately equal to 0.525. As shown in the Figure, at initial water saturation equal to 0.525, the SC_{CO_2} is around 0.475. In the drainage flow test, the brine relative permeability shows a rapid decline in brine saturation. This is due to the rapid invasion by the SC_{CO_2} which can reduce the brine hydraulic conductivity of the core sample. Hence, a gradual increase in relative permeability at drainage flow reaching 0.2 at brine saturation of 0.53. Moreover, in the imbibition flow test that is performed after the drainage flow test, the residual SC_{CO_2} was found to be 0.34. This is about 72% of the initial brine saturation. It is also observed; the imbibition flow test relative permeability results are higher than its drainage flow test. This might be due to the pore-level displacement physics which is related to the redistribution of fluids between floods (Akbarabadi & Piri, 2013).

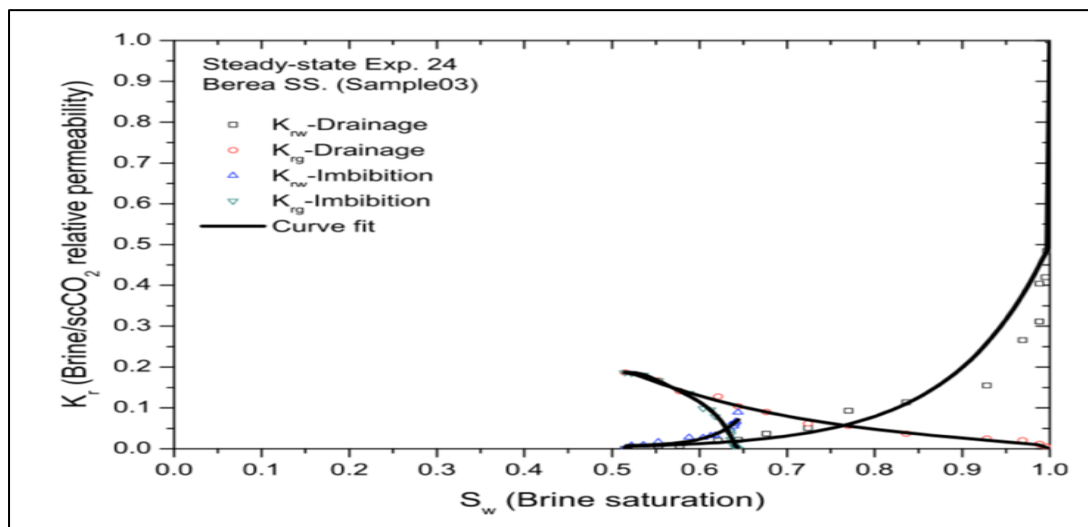


Figure 3: Relative permeability curves for sandstone core sample

2.3.1.4 Capillary Pressure

Capillary pressure is the difference in pressure across the interface between two miscible fluids. To demonstrate capillary pressure, a capillary tube contains two immiscible fluids; oil and brine. The brine will be at the bottom of the tube because the density of brine is higher than oil.

The pressure in the oil phase above the interface will be slightly greater than the pressure in the brine phase. This pressure is referred to as capillary pressure. Typically, the highest pressure coexisting in a phase is considered as a non-wetting phase (Terry & Rogers, 2014). Capillary pressure is expressed as shown below in Equation 3:

$$P_c = \frac{9.519(10^{-7})\sigma_{wo}\cos\theta}{r_c} \quad (3)$$

Where;

P_c : capillary pressure, psi

σ_{wo} : oil-brine interfacial tension, dynes/cm

θ : contact angle

r_c : radius of capillary, feet

The factors that can affect the capillary pressure in a porous medium are the chemical composition of rock and fluids, pore-size distribution of grains, and saturation of the fluid occupied in the pores. Therefore, during drainage and imbibition displacement alternative values of capillary pressure are obtained to generate the capillary pressure hysteresis and estimate the rock-fluid system (Terry & Rogers, 2014).

Numerical simulations and experimental methods are done to obtain the capillary pressure curve for the coquina rock sample, as shown in Figure 3. Primary drainage displacement of water by oil till the connate water saturation is reached. Prior to primary drainage, the rock is in water-wet condition, this is because the rock is fully saturated with brine and no oil exists in the core sample. In Figure 3, the connate water saturation (S_{wi}) obtained through the experimental method is approximately around 0.089. Good agreement is shown between the corresponding experimental and simulated capillary pressure curves (Drexler et al., 2020).

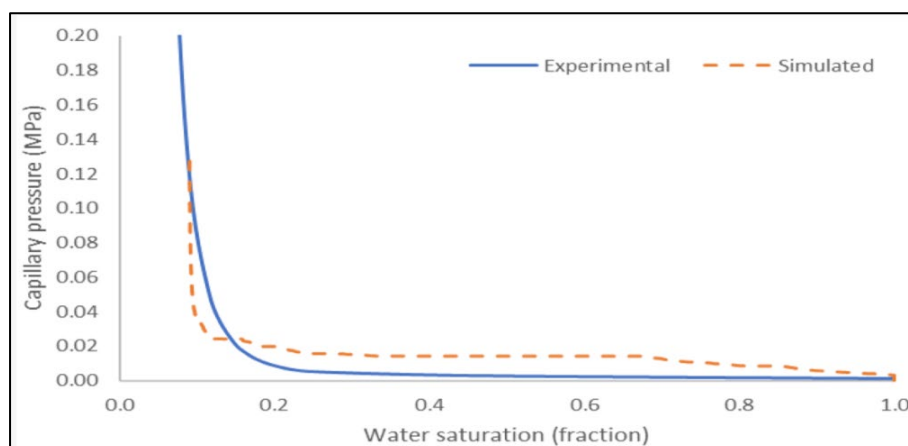


Figure 4: Capillary pressure curves for coquina sample

After drainage displacement, water is displaced by oil (imbibition displacement) to determine the residual oil saturation. As a consequence, the relative permeability curve is obtained as shown in Figure 4. Two different water were used in the experiment at drainage displacement: formation brine and carbonated brine. The purpose of using two types of different brine salinity is to study the effect of the water injection and carbonated brine injection on relative permeability curves. As shown a positive impact of carbonated brine injection on relative permeability curve. Due to the fact that the crossover point is shifted toward the higher water saturation. This indicates an increase in wettability toward the water; predominantly, increasing saturation of the wetting phase. In addition, the endpoint of the relative permeability to water is reduced in carbonated brine injection. Consequently, the injection of carbonate brine increases the flow capacity of the oil phase as observed from the obtained relative permeability curves (Drexler et al., 2020).

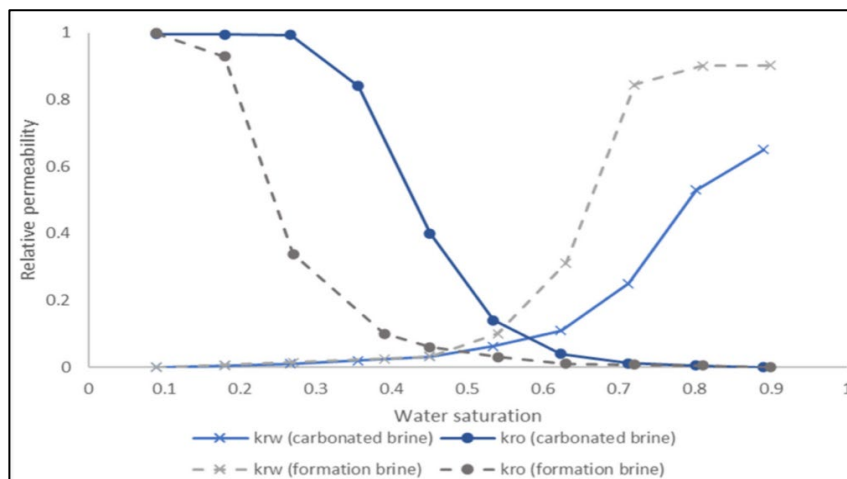


Figure 5: Imbibition relative permeability curves for coquina sample

2.3.2 Microscopic Displacement

The main factors that affect the microscopic displacement efficiency are reservoir heterogeneity and mobility of displacing phase with mobility of displaced phase (Terry & Rogers, 2014).

Reservoir heterogeneity in such variation of porosity, permeability, and clay cement can cause non-uniform flow distribution of the displacing phase. Also, in naturally fractured reservoirs, fluids will try to escape and travel through the fractures due to high permeability streaks leading to early breakthroughs leaving behind plenty of trapped reservoir fluid. Variation in both vertical and horizontal permeabilities, affect the sweep efficiency across the reservoir. Mainly, the vertical and areal efficiency will be reduced. In permeability stratification, the displacing phase sweeps faster in high permeability zones leaving behind that much of oil in less permeable zones (Terry & Rogers, 2014).

Mobility is the ratio of effective permeability to fluid viscosity. Basically, it measures how flow can flow easily through porous media. The mobility of the displacing phase is measured when the injected fluid starts to displace the oil reservoir and begins to break through at the production. Basically, it is measured the average displacing phase saturation. Whereas, the

mobility of the non-displacing phase is measured before the injection of the displacing phase. It is measured at the displacing phase saturation (Terry & Rogers, 2014).

Viscous fingering is a phenomenon that occurs when the interface of two fluids bypass zones of the reservoir creates an uneven sweep or fingered profile across the reservoir. Mainly, it occurs when the mobility of the displacing phase is greater than the mobility of the displaced phase. This subject can be resolved by the arrangement of production and injection wells which depend on the geology of the reservoir. Understanding the permeability effects and heterogeneity of the reservoir can support the planning of the arrangement of the wells to avoid poor sweep efficiency during flooding (Terry & Rogers, 2014).

2.4 CO₂ Supercritical

Supercritical CO₂ injection is considered as one method of recovering trapped oil in the reservoir. This method is categorized as a tertiary recovery technique. CO₂ can be mixed and dissolved with oil (miscible fluids) at reservoir conditions. Consequently, injection of CO₂ reduces the viscosity of oil and allows the remaining oil in the reservoir to be displaced and flow easily. The amount of recovered oil depends to a large extent on the geological reservoir conditions (pressure and temperature), and oil compositions. The main benefit of CO₂ injection is that the CO₂-produced oil can be separated and re-injected in the reservoir. Supercritical fluids are physically similar to liquids or gases. So, supercritical CO₂ density is similar to liquid phases and the mobility is more often compared to gas phases. Carbon dioxide becomes supercritical under certain temperature and pressure conditions. The temperature and pressure should be above 31.1°C and 7.38 Mpa respectively. At those conditions, the injected CO₂ is maintained in a dense state and its buoyancy in the reservoir will be reduced. Figure 6 shows the effect of temperature and pressure on CO₂ density (Whittaker & Perkins, 2013).

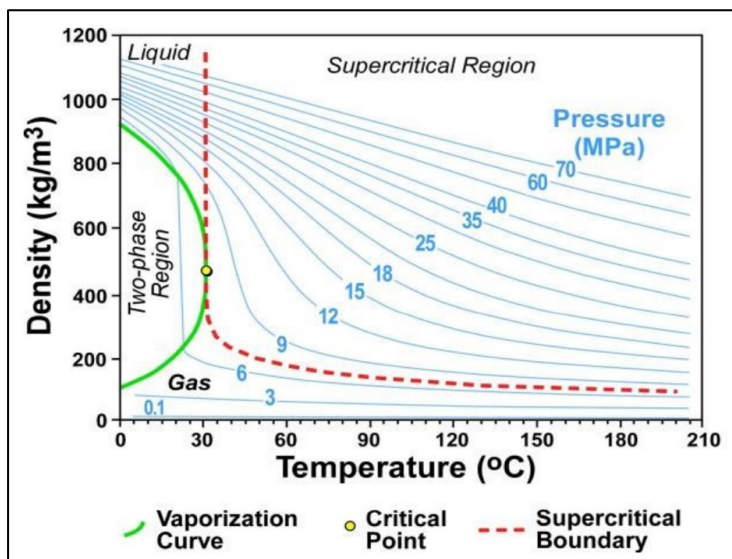


Figure 6: Density of carbon dioxide in relation pressure and temperature

During the application of CO₂ injection, dense CO₂ contacts the reservoir oil in which the CO₂ is mixed with the reservoir oil so that the oil can be dissolved. Repeated contact of CO₂ with oil can mix to become a single phase. This is because mixing between fluids oil and CO₂ does not happen instantly. This type of CO₂ flood is called miscible flooding. As mentioned earlier, miscibility can cause the oil to swell to become less viscous to enhance the mobility of the oil through the reservoir pores. In CO₂ flooding, to maintain the oil- CO₂ miscibility to achieve an effective outcome which increases the oil recovery. Therefore, Minimum Miscibility Pressure (MMP) needs to be identified and confirmed through laboratory analyses for any particular reservoir. Usually, during CO₂ flooding, the design is implemented at a condition where reservoir pressure is above the MMP. In case the pressure during the flooding operation dropped below MMP, lighter hydrocarbon components in the oil will be produced which might cause the residual oil to be more viscous and difficult to recover at a further stage. Typically, producing lighter components of the oil will increase the potential of asphaltene and waxes to be formed and precipitated in the reservoir. As discussed earlier, precipitation of heavy hydrocarbons can plug the pores and small connecting channels of the reservoir (Whittaker & Perkins, 2013).

The density of supercritical CO₂ is slightly lower than oil and water, so the buoyancy effect will be established in the reservoir as CO₂ is injected. This will provide a smooth front of CO₂ to sweep the trapped oil in the reservoir. The main factors that affect the sweeping efficiency of CO₂ distribution are porosity and permeability. Reservoir heterogeneity plays a major role in sweep efficiency. Therefore, in reservoirs with small-scale heterogeneities, CO₂ will disperse and increase the contact region between CO₂ and oil. Hence, at larger scale heterogeneities, may channel the CO₂ flow path in which reservoir sweep will be reduced. Basically, in CO₂ flooding modeling, the reservoir heterogeneities, relative permeability, and wettability need to be studied and analyzed to determine the CO₂ injection rates, sweeping efficiency, and reservoir pressure management (Whittaker & Perkins, 2013).

Chapter 3: Methodology

3.1 Core Cut Machine

It is essential to have the cylindrical shape of the core sample of the rock before the experiment. A machine is used to cut the core taken from the side of drilled well into a perfect shape. This machine is from the “Wiltion” company, it can cut the rock into cylindrical core samples for experimental analysis. The typical measured diameter and length of the core sample are 1 inch and 3 inches respectively.

3.2 Cleaning Samples (Stark and Dean Method)

Four carbonate–limestone core samples were selected from a well in Bu Hasa field. The four core samples used in the experiment namely, 9A, 12A, 13A, and 14A. Figure 7 shows the core samples where minor vuggs are shown. The first step of the experiment is to clean the core samples through the Soxhlet system. Toluene fluid is used to extract the hydrocarbons saturated within the cores. Whereas, methanol vapor is used to extract salts from the core sample. After, leaving the cores in the system for two to three days, the cores are fully empty with no fluid occupied.



Figure 7: Experimental core samples

Afterward, the samples were taken to the oven to dry the samples. When using the equipment, it is necessary to set the time that you want the oven to work at. Also, ensure the window of the oven is closed. After the setting time, open the oven and check the core samples are dried. In case, the samples are still wet, then set another time to completely dry the samples. Accordingly, once the core samples are dried, it means the core samples are clean now and the weight of each sample can be measured to know the dry weight.

3.3 Core Dimensions

The length and the diameter of four carbonate core samples were measured using a caliper instrument. Three different measurements were taken for length and diameter. Then, the average length and diameter for each sample were measured. Table 1 shows the average length and diameter of the four samples.

Table 1: Core sample dimensions

Core Sample ID	Length (cm)	Diameter (cm)
9A	5.156	3.812
12A	4.970	3.811
13A	5.106	3.809
14A	5.091	3.809

3.4 Liquid Permeability and Porosity Measurements

The Poro-Perm apparatus is designed to measure the porosity and permeability of a core sample. To measure the porosity of the core sample, nitrogen gas is pumped into the dry core sample to measure the pore volume of the sample. The average diameter and length as well as dry weight of the sample is entered into the software. As the pore volume is determined for each core sample, the porosity is measured using Equation 4.

$$\emptyset = \frac{V_p}{V_b} \times 100 \quad (4)$$

Where;

\emptyset : porosity; %

V_p : pore volume; cubic centimeter

V_b : bulk volume; cubic centimeter

Moreover, the permeability of the core sample is measured by injecting nitrogen gas into the core sample and applying overburden pressure to 400 psi. Differential pressure across the core sample is monitored till it stabilizes. The permeability of the core sample to N₂ gas is given by the software. Porosity and permeability for each core sample are shown below in Table 2.

Table 2: Rock properties of core samples

Core Sample ID	Porosity Air (%)	Porosity Water (%)	Permeability (mD)
9A	16.79	10.71	28.70
12A	13.68	8.43	30.07
13A	13.66	5.80	35.60
14A	17.00	14.54	64.08

3.4 Brines Preparation

The initial stage prior to brine saturation is to prepare the brine at different salinity. Four different brine salinities were prepared for four different core samples. Raw Sodium Chloride (NaCl) and water were stirred and mixed together to achieve the required salinity. Different grams of Sodium Chloride were mixed with respective liters of water as shown in Table 3. Later on, a pycnometer is used to measure the density of the prepared brine. The pycnometer density is 50.1067 mL. Moreover, Figure 8, shows the experiment conducted to prepare the grams of

Sodium Chloride (NaCl) to be poured into the water and stirred. Below is the procedure implemented to prepare the brines:

- 1- Prepare NaCl salt as per the respective salinity of the brine as shown in Table 3.

Table 3: Brine salinity for each core sample

Core Sample ID	Proposed salinity (ppm)	NaCl salt (grams)
9A	50,000	100
12A	100,000	150
13A	200,000	200
14A	250,000	250

- 2- Add 1 Liter of distilled water into container. Place the funnel above the container and add the salt.
- 3- Stir the mixture (salt & distilled water) and wait till homogenous fluid is achieved.



Figure 8: Brine mixing apparatus

- 4- Perform degassing for the brine using hose and vacuum pump.
- 5- Place the prepared brine in a container and write the brine's name.

3.5 Vacuum and Pressure Method Saturation

The purpose of this experiment is to saturate the core samples with different brine salinity. The vacuum and pressure method was used to evacuate and saturate core samples with brine. The equipment used in this experiment is Saturator. This experiment is done prior to capillary pressure

measurement as well as carbon dioxide (CO₂) flooding. The core is placed inside the cylinder to saturate the core sample with brine at respective salinity under pressure. A vacuum pump is attached to the cylinder to extract air occupied in the core sample. After that, saturating pressure is applied to saturate the core sample fully with brine. Figure 9 shows the Core Saturator equipment.

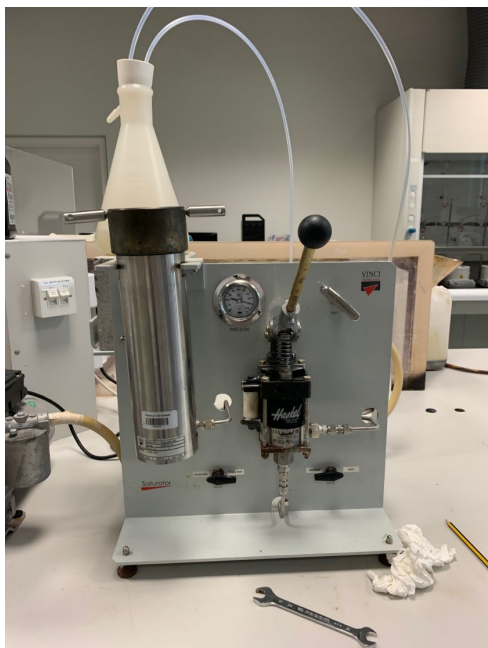


Figure 9: Vacuum and pressure apparatus

3.6 Porous Plate Technique

The porous plate technique is a method used to desaturate the core sample by displacing brine into the air under pressure. The purpose of this method is to measure the irreducible water saturation (S_{wirr}) and capillary pressure. Initially, each core sample is fully saturated with brine in which the weight of the sample is known. The desaturation stage starts by placing all the core samples into the porous plate and setting the pressure to 3 psi. Every twenty-four hours, the weight of the core samples was measured till the weight of each sample is stabilized. Then, the desaturation continues by increasing the pressure in stages and the sample is weighted to

determine the loss of brine. This technique is continued till 106 psi at which no more weight loss is observed. The state at which no more brine can be displaced from the core sample is called irreducible water saturation.

3.7 Carbon Dioxide Flooding

In this research, CO₂ was used in the experiment to flood four core samples with different brine salinity systems. The conditions of CO₂ flooding are shown below in Table 4. During the experiment, CO₂ is being injected at the supercritical phase at which temperature and pressure should be above 31.1°C and 7.38 Mpa respectively. The flooding conditions were conducted at different temperatures yet, at constant injection pressure.

Table 4: CO₂ flooding conditions

Condition	Flooding 1	Flooding 2	Flooding 3	Flooding 4
Core sample ID	9A	12A	13A	14A
Brine salinity (ppm)	50,000	100,000	200,000	250,000
Temperature (Fahrenheit)	150	200	250	300
Injection pressure (psi)	1270	1270	1270	1270

Chapter 4: Experimental Results

In this section of the report, the main findings obtained from laboratory experiments will be elaborated on and shown. The results include capillary pressure curves of different brine systems, pore size distribution, CO₂ relative permeability curves, and experimental CO₂ flooding tests. Also, this section of the report include simulation runs that were conducted for different temperature, gas-specific gravity, and brine viscosity to obtain the brine recovery and CO₂ storage factor. Therefore, based on the results obtained a detailed description will be provided to explain the flow mechanism of the CO₂/Brine system.

4.1 Capillary Pressure

Based on the porous plate experiment conducted, Tables 8 – 11 in Appendix A shows the pump pressure and brine weight loss for four core samples. As shown, the maximum pump pressure to be reached using a porous plate is 106 psi. Therefore, at 106 psi, the irreducible brine saturation (S_{wirr}) is achieved. Moreover, Figures 10 – 13 show the capillary pressure curves for four core samples at the drainage flow experiment where air displaces brine.

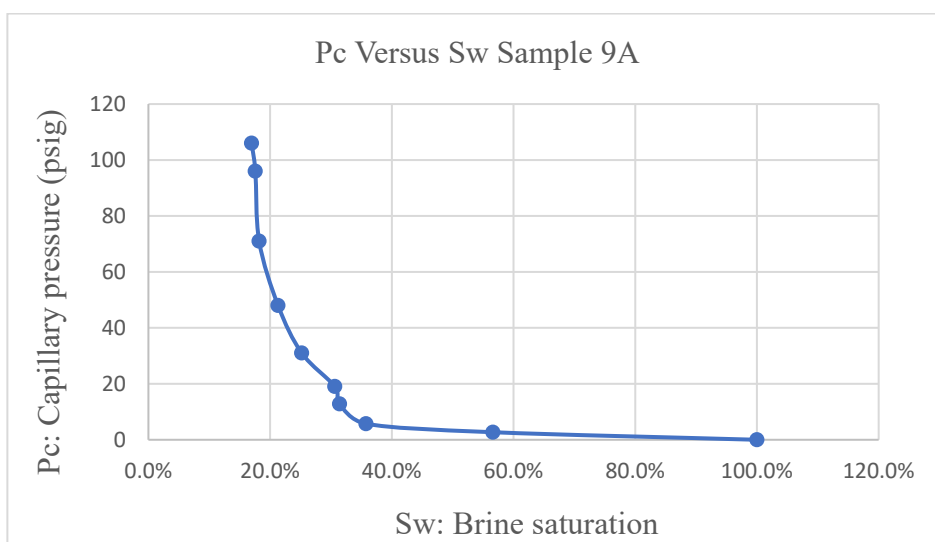


Figure 10: Primary drainage capillary pressure curve at 50,000 ppm brine salinity

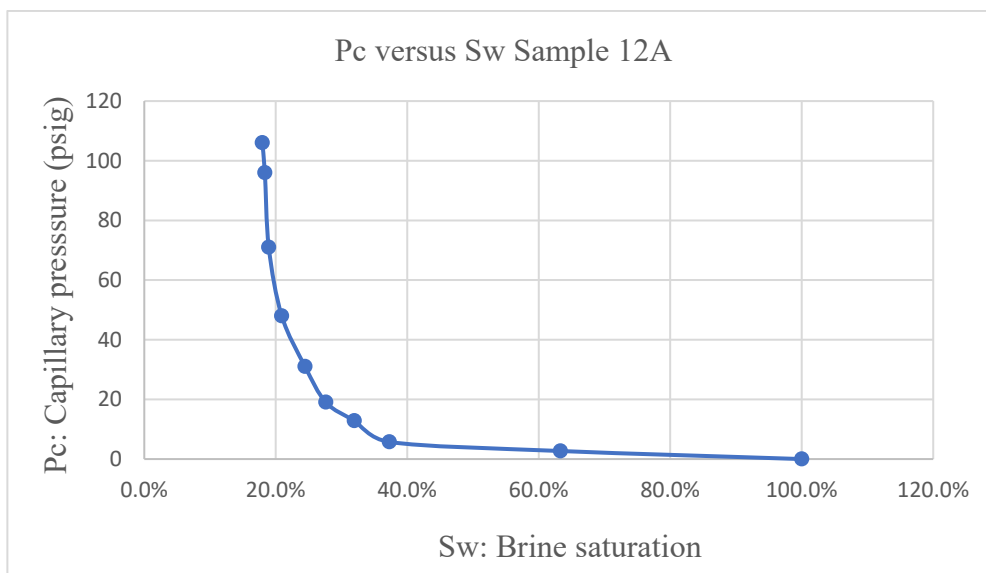


Figure 11: Primary drainage capillary pressure curve at 100,000 ppm brine salinity

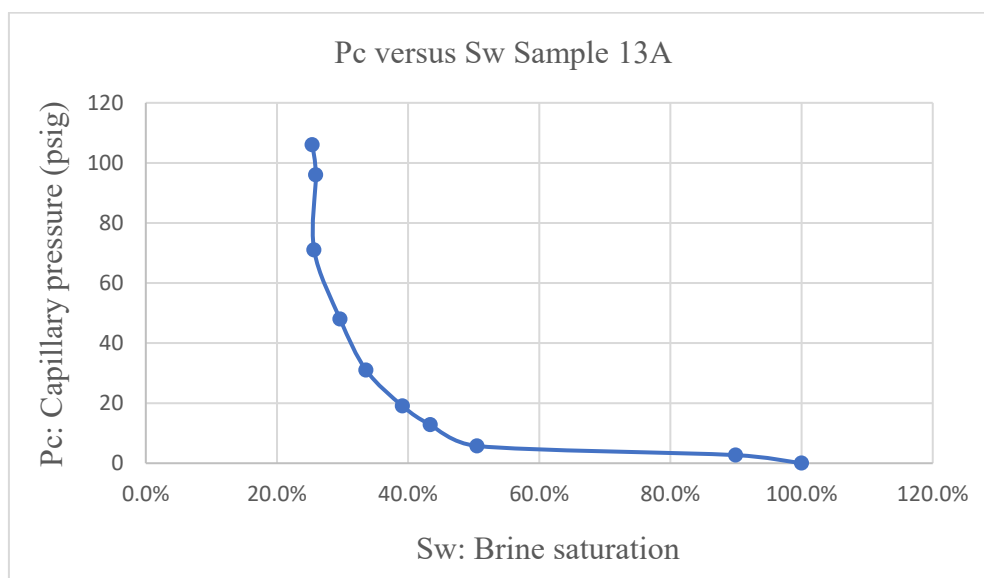


Figure 12: Primary drainage capillary pressure curve at 200,000 ppm brine salinity

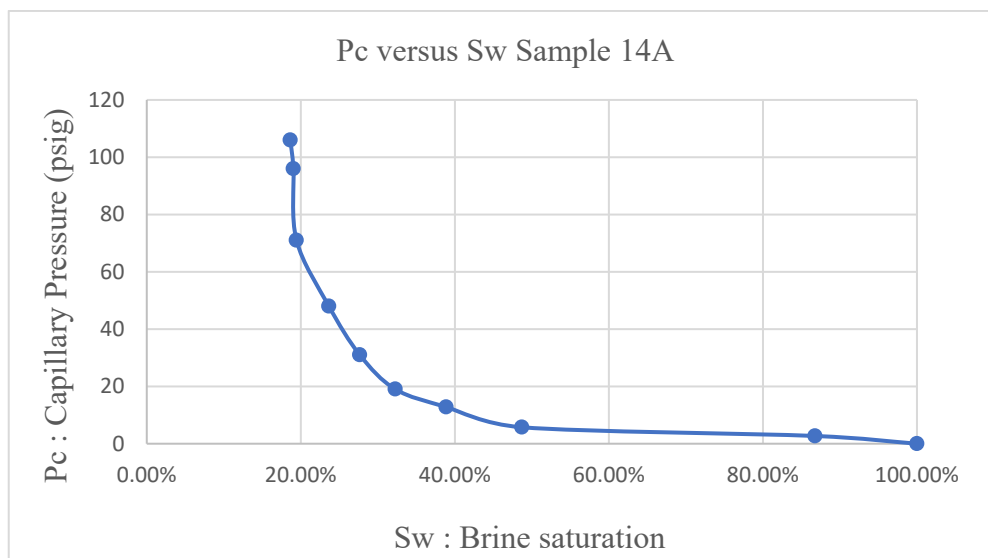


Figure 13: Primary drainage capillary pressure curve at 250,000 ppm brine salinity

4.1.1 Pore Size Distribution

To validate the results of capillary pressure obtained from a laboratory experiment, a pore size distribution technique is conducted. Using capillary pressure curves, an approximate pore size distribution of rocks can be obtained if one of the phase fluids is non-wetting. A rock is composed of a variety of interconnected pore throat sizes and pore volumes occupied in the pores. Therefore, the distribution across the formation is an important property that needs to be analyzed during fluid transport in porous media.

Ritter and Drake's model was used to identify the pores size distribution for each sample. The model represents the invasion of the non-wetting phase into porous media. Burdine et al. modified the model and used mercury-injection capillary pressure curves to provide a model representing the distribution of the pore. Equation 5 is used to calculate the pore size distribution (Tiab & Donaldson, 2012). As shown, the pore throat size distribution, $D(r_i)$ is a function of pore throat radius (R_i). Figures 14 – 17 show the size of the distribution of the pores for each sample. Refer to Appendix B for the pore size distribution results.

$$D_{(ri)} = \left(P_c \times \frac{V_p}{r} \right) \left(\frac{dS_w}{dP_c} \right) \quad (5)$$

Where;

$D_{(ri)}$: is the pore size distribution, meters square

P_c : capillary pressure, dynes/cm³

V_p : pore volume, cm³

r : pore radius, microns

dS_w/dP_c : hyperbola derivative of inlet saturation and inlet capillary pressure, dynes/cm³

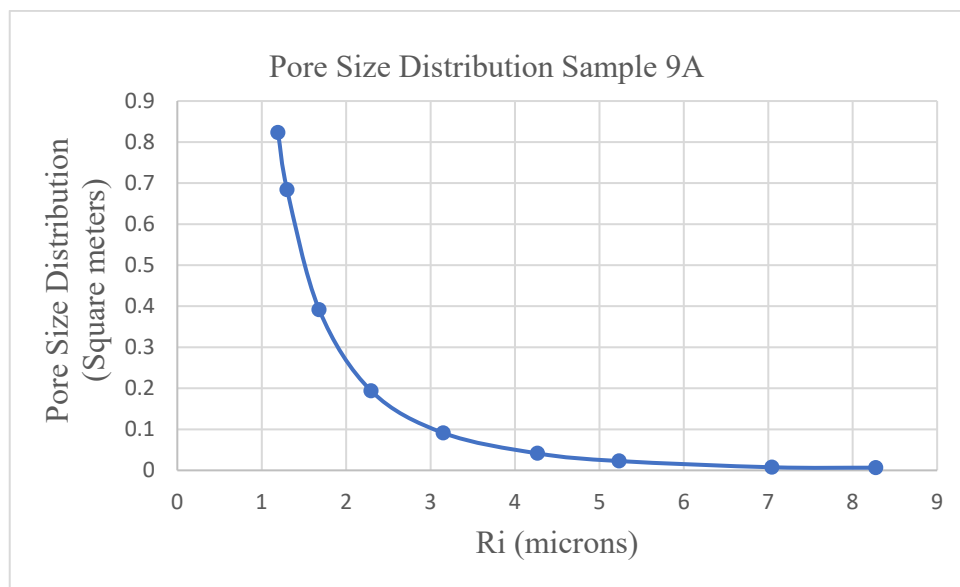


Figure 14: Pore entry size distribution for core sample 9A

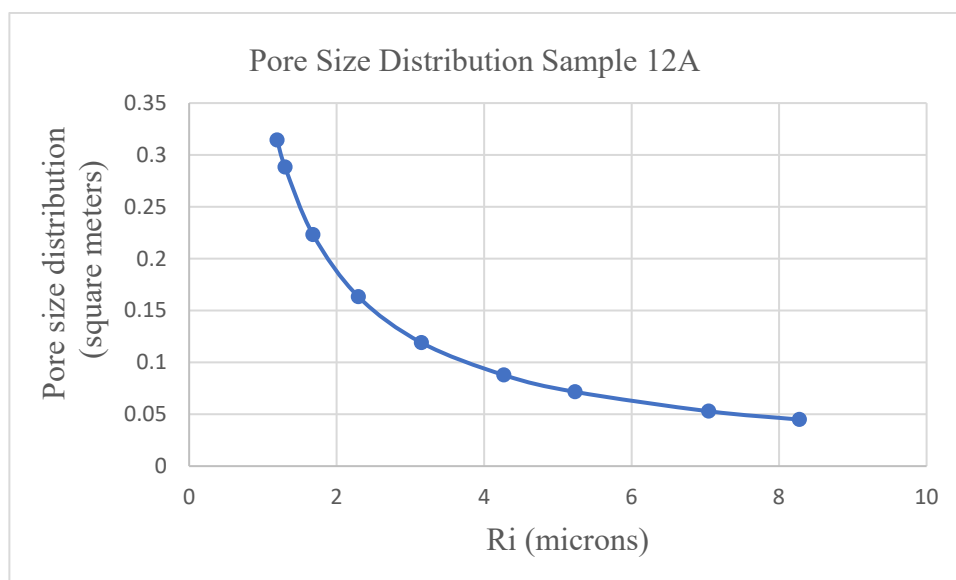


Figure 15: Pore entry size distribution for core sample 12A

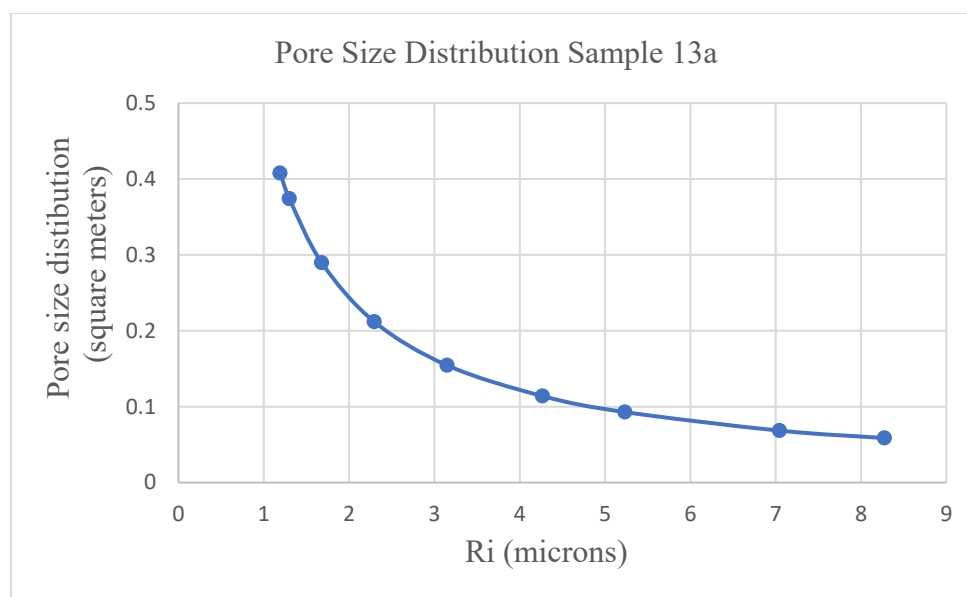


Figure 16: Pore entry size distribution for core sample 13A

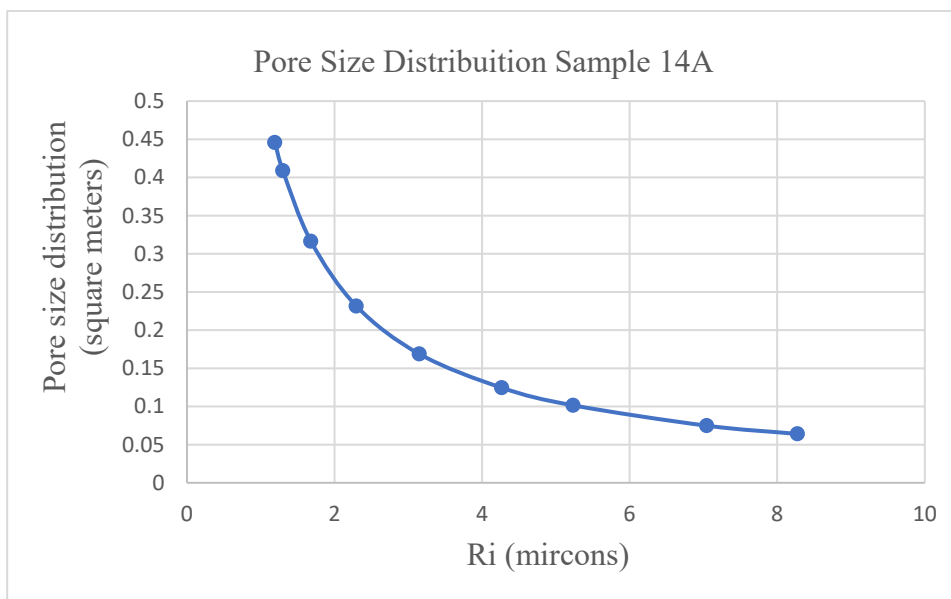


Figure 17: Pore entry size distribution for core sample 14A

4.2 Relative Permeability

During CO₂ flooding into fully brine saturated core samples, the volume of displaced water was measured. Additionally, the water and CO₂ saturation were obtained. The time and volume of gas (CO₂) breakthrough achieved is recorded. Carbon dioxide (CO₂) breakthrough is when the injected CO₂ starts producing from the core sample. After the breakthrough, CO₂ and brine are produced together till the saturation ratio of CO₂ starts to rise until no more CO₂ is capable to displace the brine out of the core sample. The time at which no more CO₂ is produced from the core sample represents the residual CO₂ saturation. This can be defined as when the CO₂ becomes immobile to displace the brine from the core sample. As shown below in Table 5, the residual CO₂ saturation for each respective sample. Refer to Appendix C for the results of the CO₂ flooding test.

Table 5: Residual CO₂ saturation obtained during CO₂ flooding test

Core Sample ID	Residual CO ₂ saturation, S _{rcO2} (%)
9A	81.9
12A	67.9
13A	72.3
14A	73.5

Moreover, to establish the relative permeability curve using Darcy's Law it was required to measure the volume of CO₂ produced, yet the volume was not recorded due to the unavailability of the gasometer. Therefore, it was proposed to use the Brooks-Corey model to identify the brine and CO₂ relative permeability. Power Law function which is similarly Brooks-Corey model, was used to obtain the relative permeability curves. Equation 6 describes the power-law function of the Brooks-Corey model (Kim et al., 2018).

$$K_{rw} = (S_e)^{N_w} \text{ and } K_{rco2} = (1 - S_e)^{N_{co2}} \quad (6)$$

Where K_{rw} is the brine relative permeability and K_{rco2} is the CO₂ relative permeability in Milli darcies. The saturation parameter (S_e) was obtained using Equation 7. N_w and N_c are exponent coefficients for water and CO₂ respectively. The typical value of N_w and N_c used in carbonate limestone reservoirs are 2.1 and 1.2 respectively (Kim et al., 2018).

$$S_e = \frac{S_l - S_{rl}}{S_{max} - S_{rl}} \quad (7)$$

Where; S_l is liquid saturation, S_{rl} is residual liquid saturation, and S_{max} is the maximum liquid saturation.

Based on the relative permeability obtained for each sample, the carbon dioxide (gas) relative permeability (K_{rco2}) endpoint was identified at critical brine saturation. Obtain the carbon dioxide (gas) relative permeability at the minimum saturation for the brine to become

mobile. Figures 18 – 21 show the relative permeability curves for the four core samples. Moreover, CO₂ relative permeability endpoints were obtained using Petroleum Solution software which provides comprehensive reservoir and EOR analysis. The endpoint value of carbon dioxide (gas) relative permeability (K_{rco2}) and different CO₂ injection temperature were considered as input data into the software. Based on the software run, the data obtained in each cumulative time were: CO₂ injection rate, water, and CO₂ production rates, storage factor as well as CO₂:Water ratio. The results of the simulator runs are shown in Appendix C for each flooding test at different temperatures. Moreover, Figures 22 – 24 represent the relationship between the rate, CO₂ cut, and cumulative time in days.

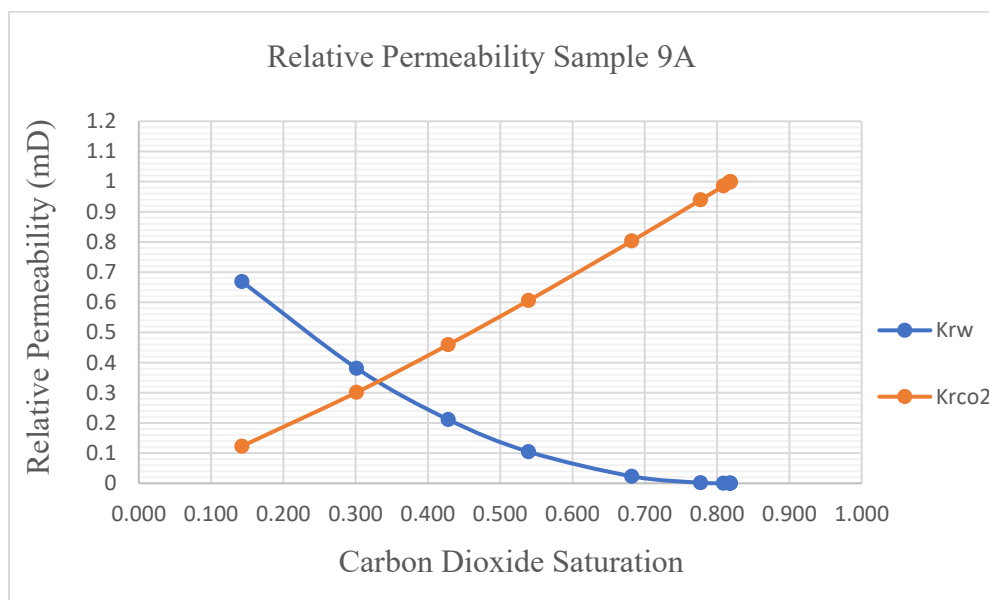


Figure 18: Relative permeability curve for core sample 9A

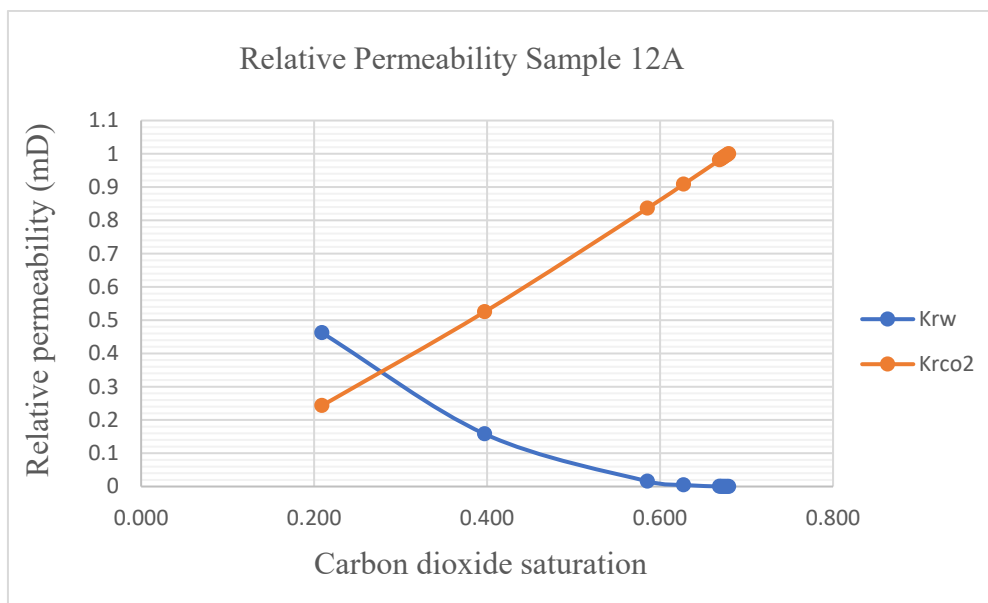


Figure 19: Relative permeability curve for core sample 12A

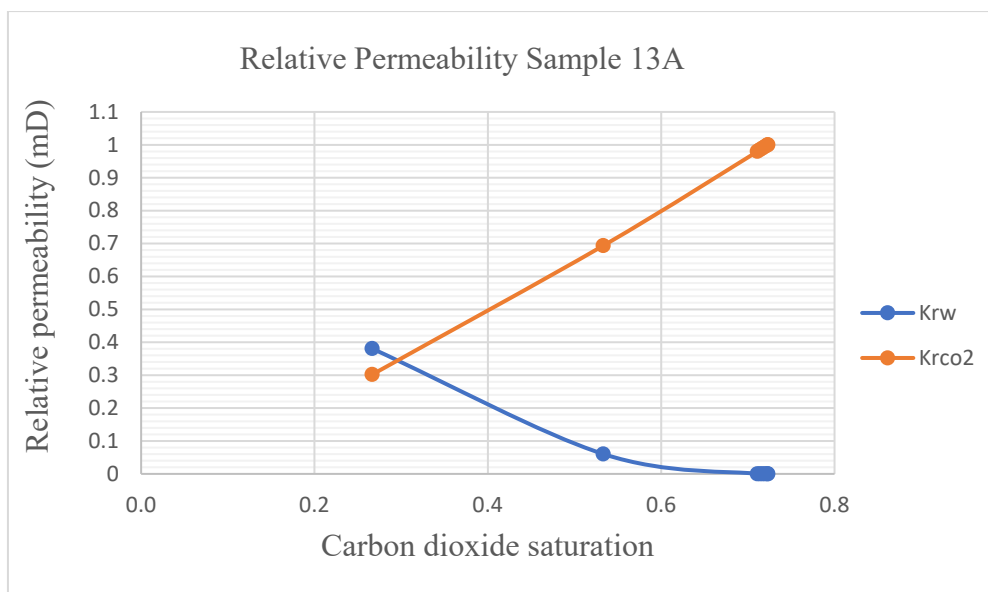


Figure 20: Relative permeability curve for core sample 13A

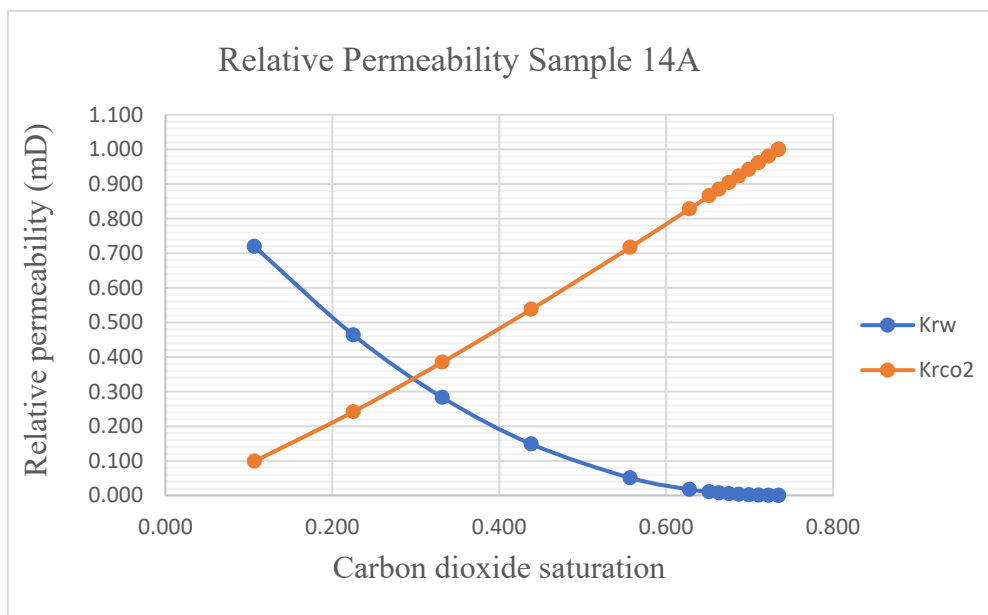


Figure 21: Relative permeability curve for sample 14A

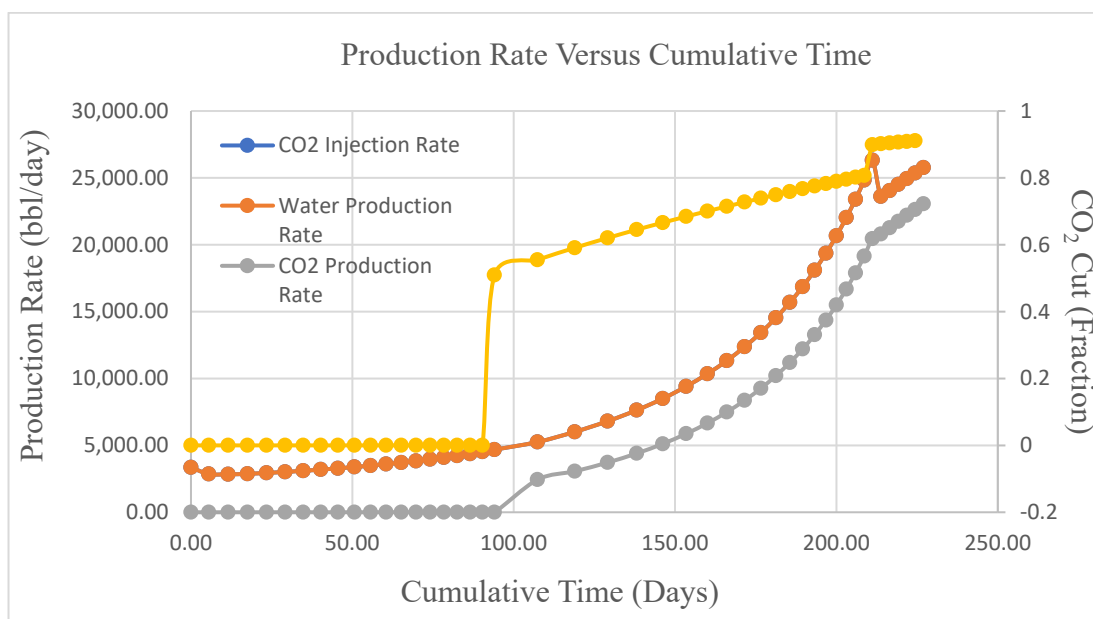


Figure 22: Production rate vs. cumulative time at 200°F

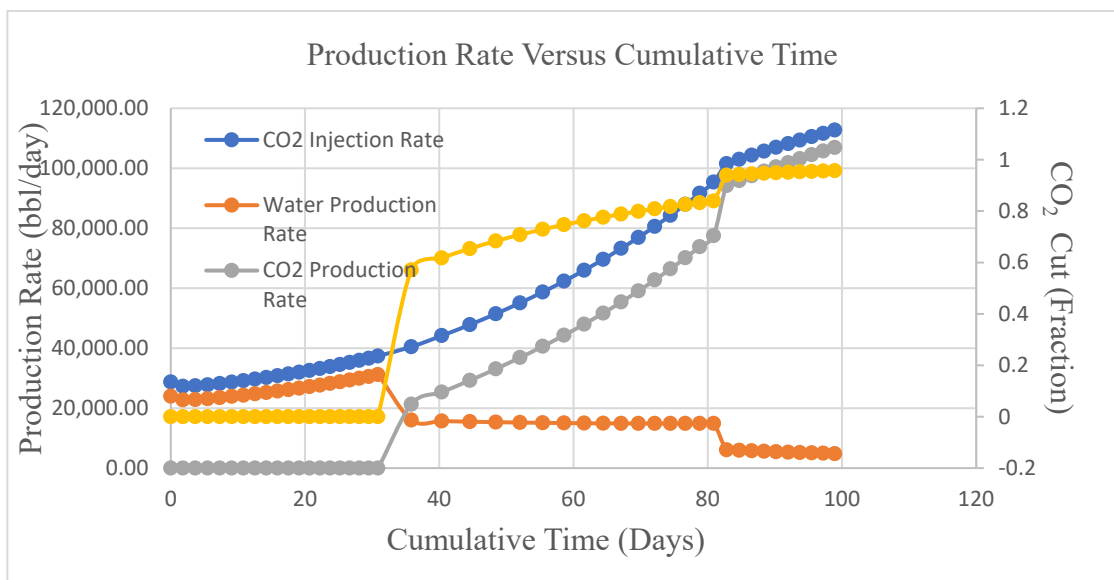


Figure 23: Production rate vs. cumulative time at 300°F

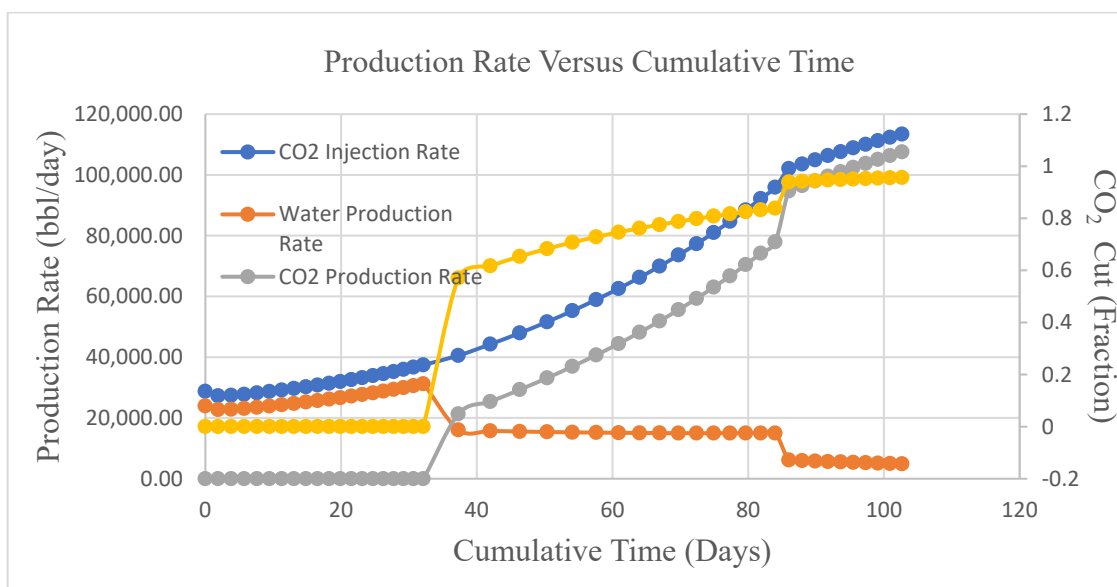


Figure 24: Production rate vs. cumulative time at 350°F

4.3 CO₂ Storage Factor

Reservoirs can be used for large-scale CO₂ storage to reduce greenhouse gas released into the atmosphere. Underground storage is the easiest and cheapest mitigation strategy taken for CO₂ disposal. Rock properties affect the storage of CO₂ in the formation. Rock formation void space

should provide the capacity to store CO₂ underground. Also, formation passage allows CO₂ to spread within the formation at the injected rate. Other factors could also affect the storage of CO₂ underground. Therefore, using CO₂ relative permeability endpoints obtained through the Brooks-Corey model, multiple simulation runs were conducted to determine the effect of temperature, gas specific gravity, and brine viscosity on CO₂ storage factor. Using Equation 8, CO₂ pore volume injected was calculated for each case scenario so that conclusions can be drawn.

$$CO_2 \text{ Pore volume injected } (ft^3) = \frac{\text{Cumulative CO}_2 \text{ injection (bbl)}}{\text{Pore volume } (ft^3)} \quad (8)$$

4.3.1 Temperature

Petroleum solution software was used to carry out CO₂ flooding of an aquifer run to illustrate the relationship between CO₂ pore volume injected and CO₂ storage factor. Using the obtained CO₂ relative permeability endpoints, the temperature effect on the CO₂ storage factor was obtained at three different temperatures: 200, 300, and 350. Figures 25 – 27 show the relationship between CO₂ pore volume injected and CO₂ storage factor at different temperatures. In addition, as shown in Figures 28 – 29 the maximum obtained CO₂ storage factor was plotted for different temperatures as well as the CO₂ storage factor at breakthrough.

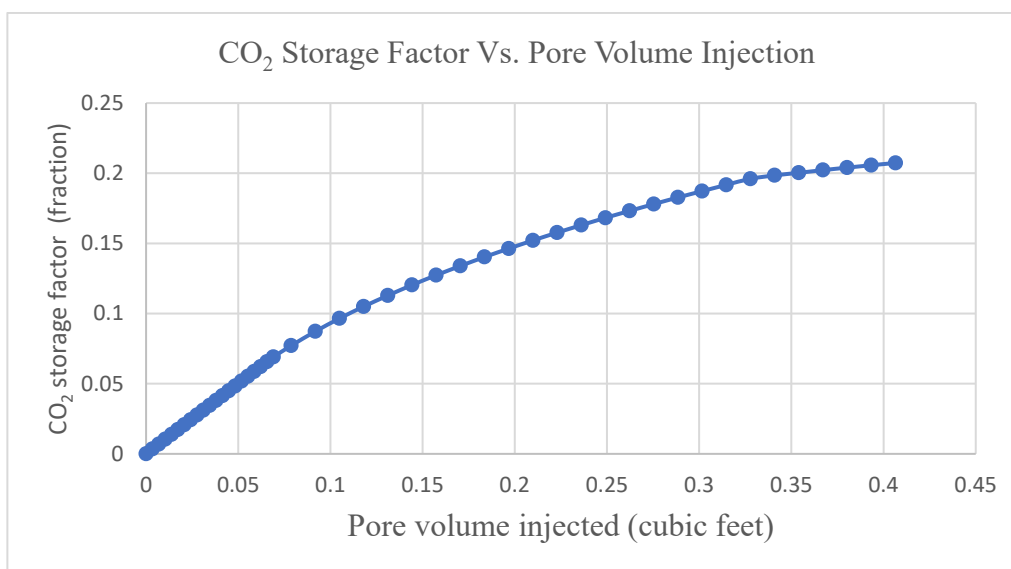


Figure 25: CO₂ storage factor versus pore volume injected for 200°F

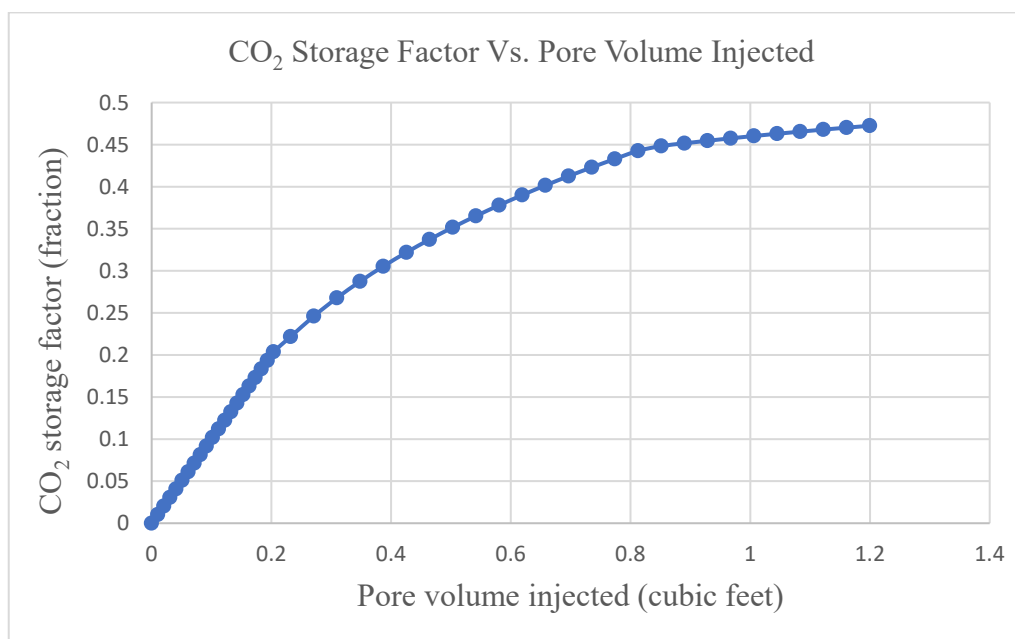


Figure 26: CO₂ storage factor versus pore volume injected for 300°F

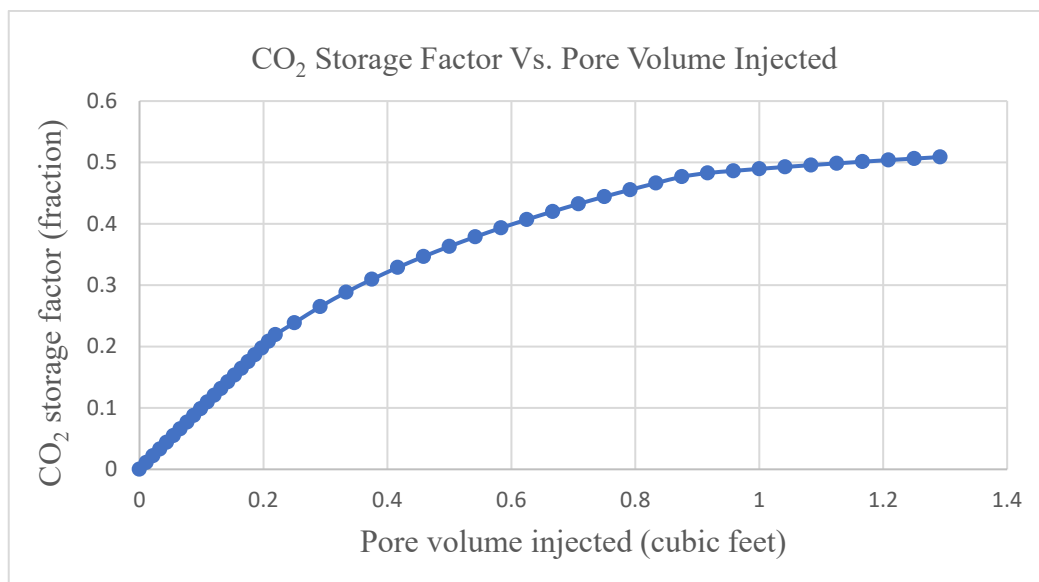


Figure 27: CO₂ storage factor versus pore volume injected for 350°F

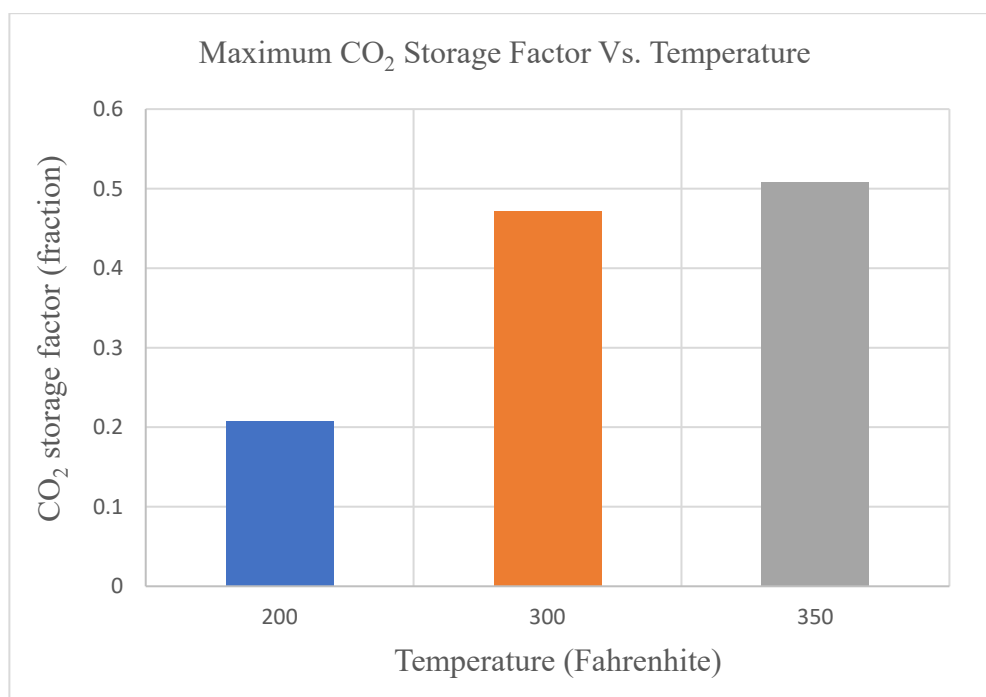


Figure 28: Maximum CO₂ storage factor at each temperature

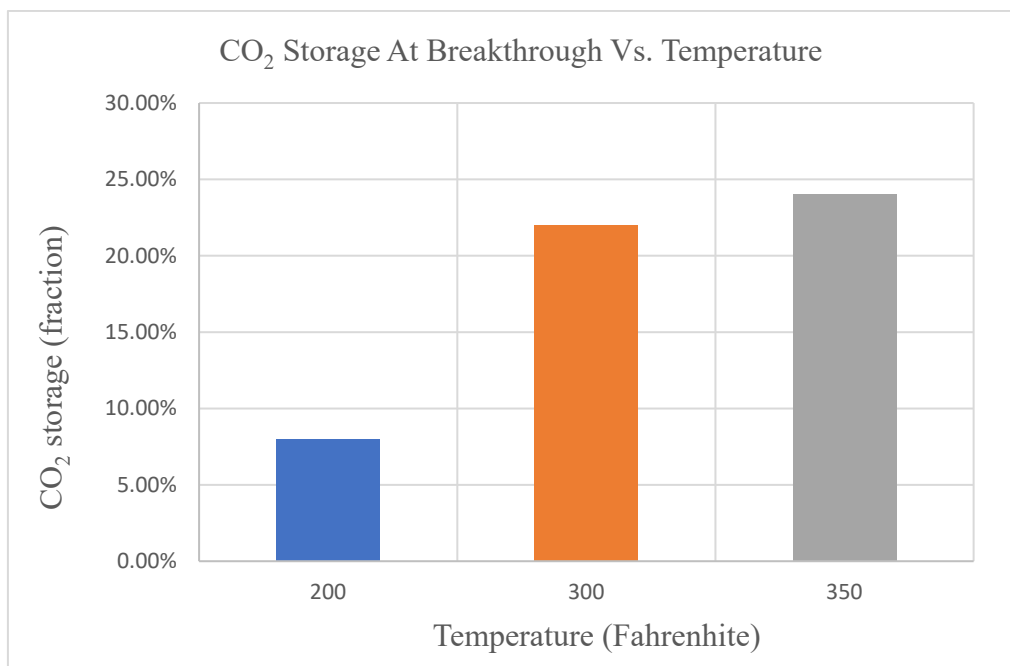


Figure 29: CO₂ storage factor at breakthrough at each temperature

4.3.2 Initial Gas Saturation

The effect of free hydrocarbon gas saturation that might exist in brine formations will be studied in this section. CO₂ flooding of aquifer runs was carried out at different gas saturation (S_{gi}) using the CO₂ relative permeability endpoints. Therefore, the CO₂ pore volume injected was calculated based on the results of the computer runs for each initial hydrocarbon gas saturation employed in this study. Figures 30 – 33 show the relationship between the pore volume of CO₂ injected and the CO₂ storage factor. Also, Figures 34 – 35 demonstrate the maximum storage factor as well as the CO₂ storage factor at breakthrough for each selected initial HC gas saturations condition.

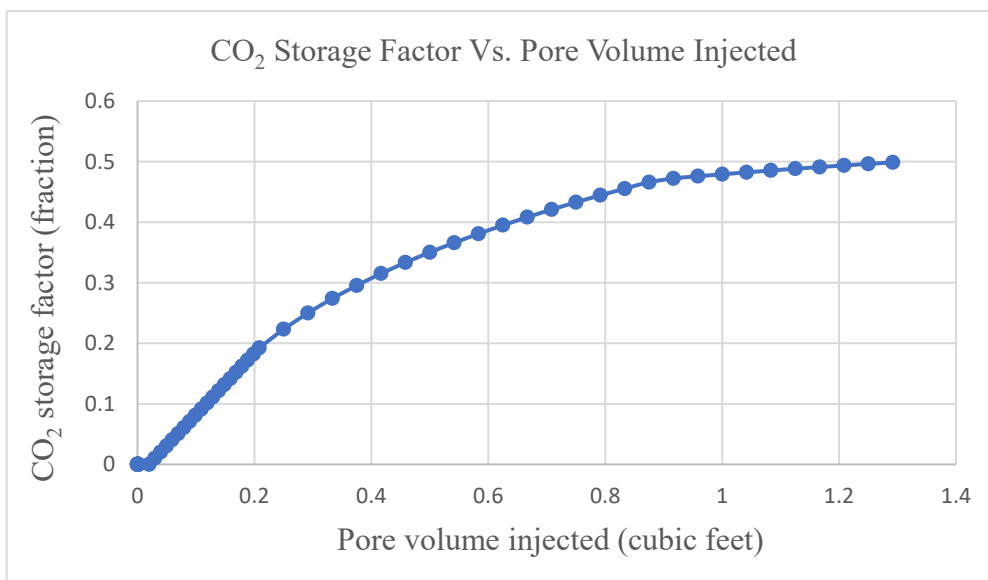


Figure 30: CO₂ storage factor versus pore volume of CO₂ injected for $S_{gi} = 2\%$

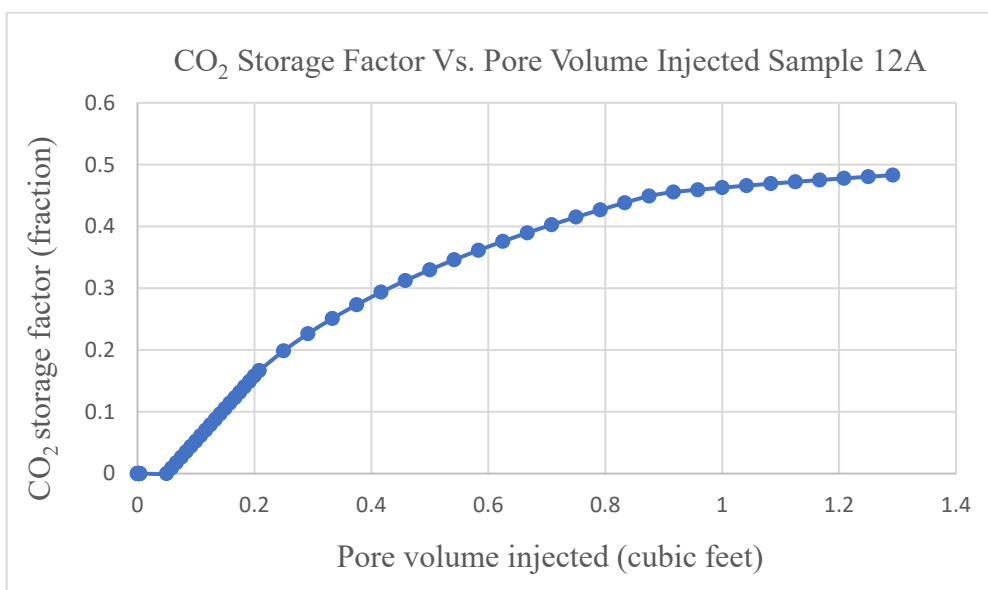


Figure 31: CO₂ storage factor versus pore volume injected for $S_{gi} = 5\%$

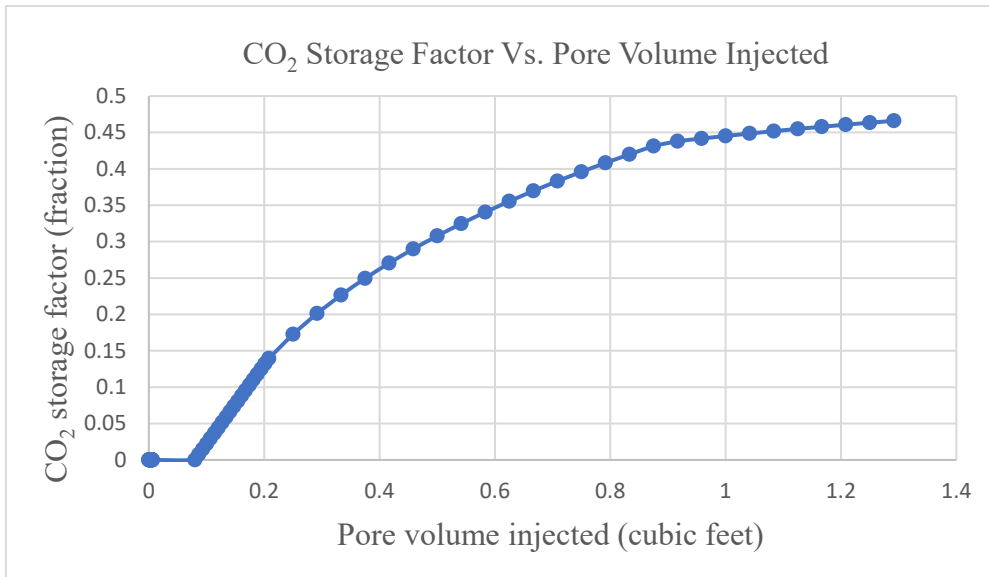


Figure 32: CO₂ storage factor versus pore volume injected for $S_{gi} = 8\%$

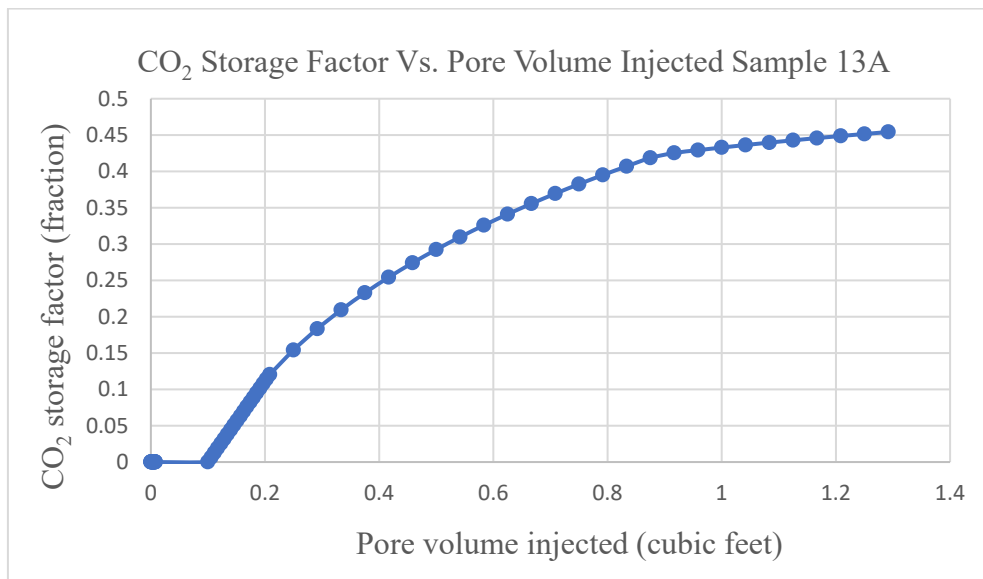


Figure 33: CO₂ storage factor versus pore volume injected for $S_{gi} = 10\%$

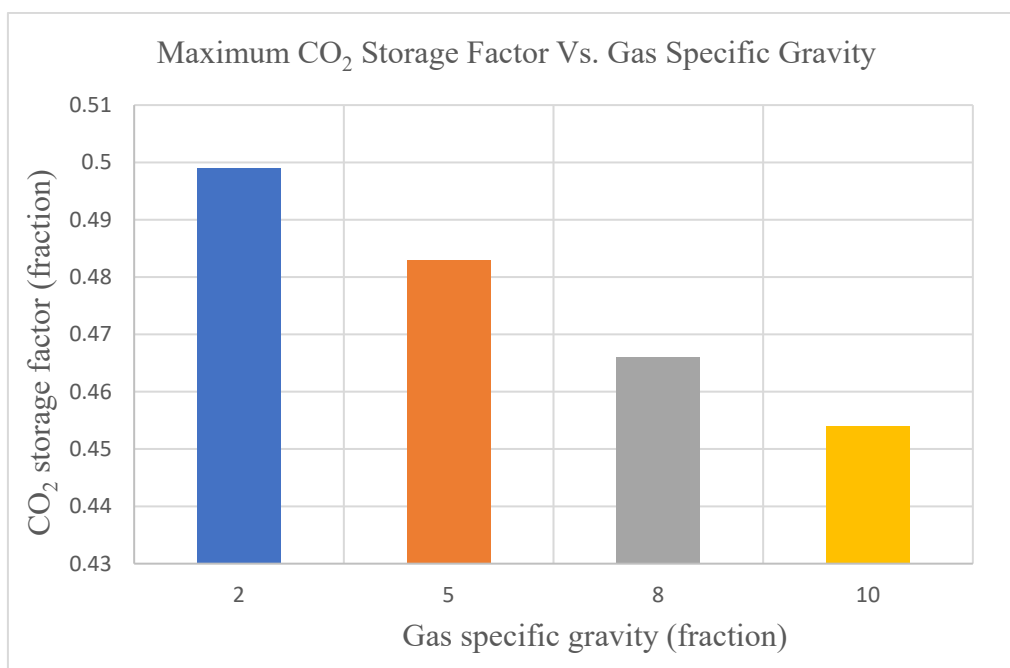


Figure 34: Maximum CO₂ storage factor at each initial HC gas saturation

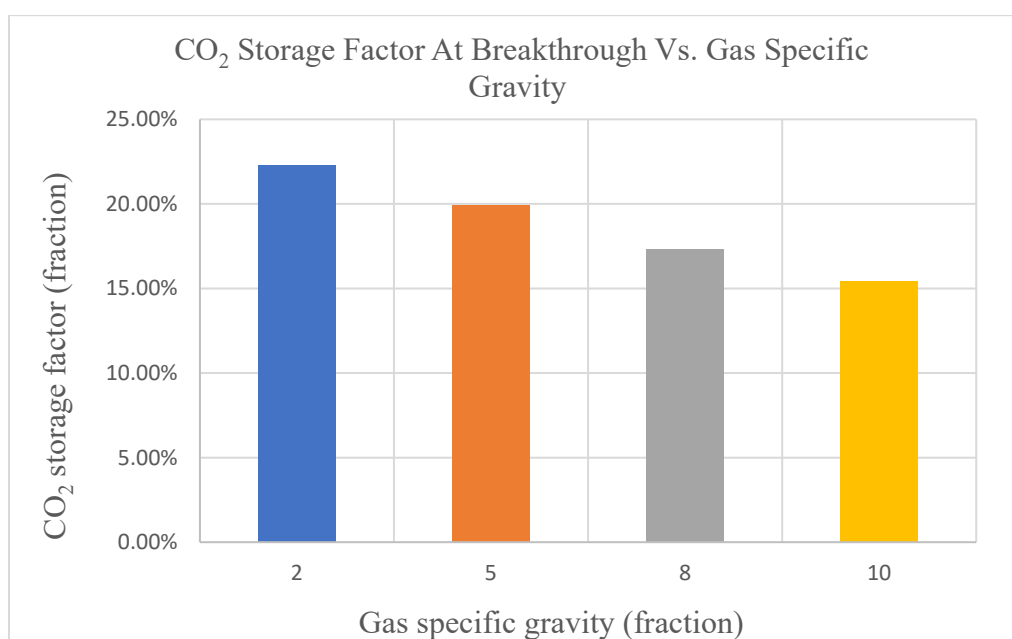


Figure 35: CO₂ storage factor at breakthrough at each HC initial gas saturation

4.3.3 Brine Viscosity

Four different brine viscosities were selected to generate software CO₂ flooding of an aquifer run using CO₂ relative permeability endpoints. CO₂ pore volume injected was calculated for four different brine viscosities to determine the relationship between brine viscosities on CO₂ storage factor as shown in Figures 36 – 39. Additionally, to demonstrate the effect of brine viscosity on the CO₂ storage factor, the maximum storage factor, as well as the CO₂ storage factor at breakthrough for each brine viscosity, are shown in Figures 40 – 41.

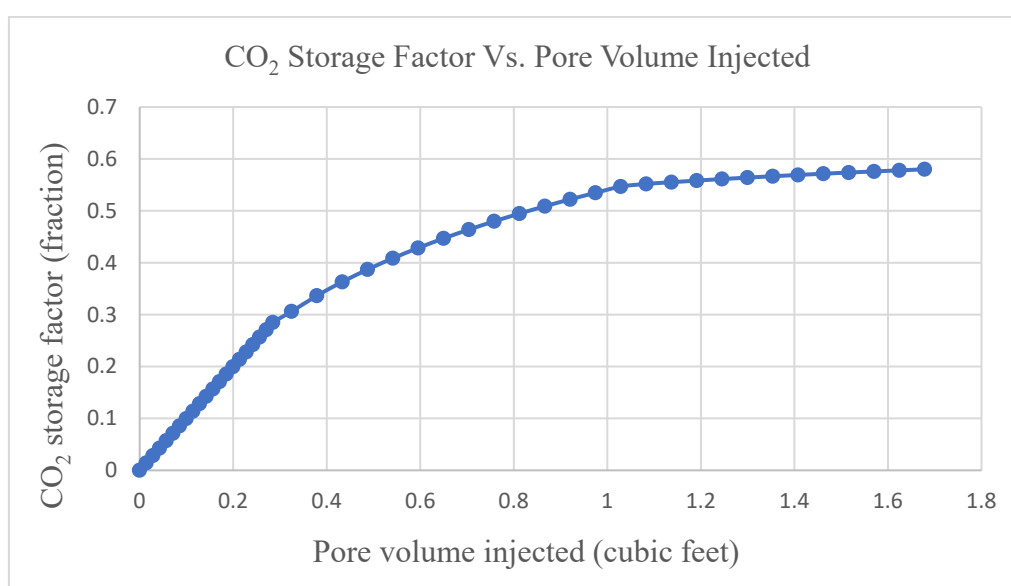


Figure 36: CO₂ storage factor versus pore volume injected for 0.1 cp brine viscosity

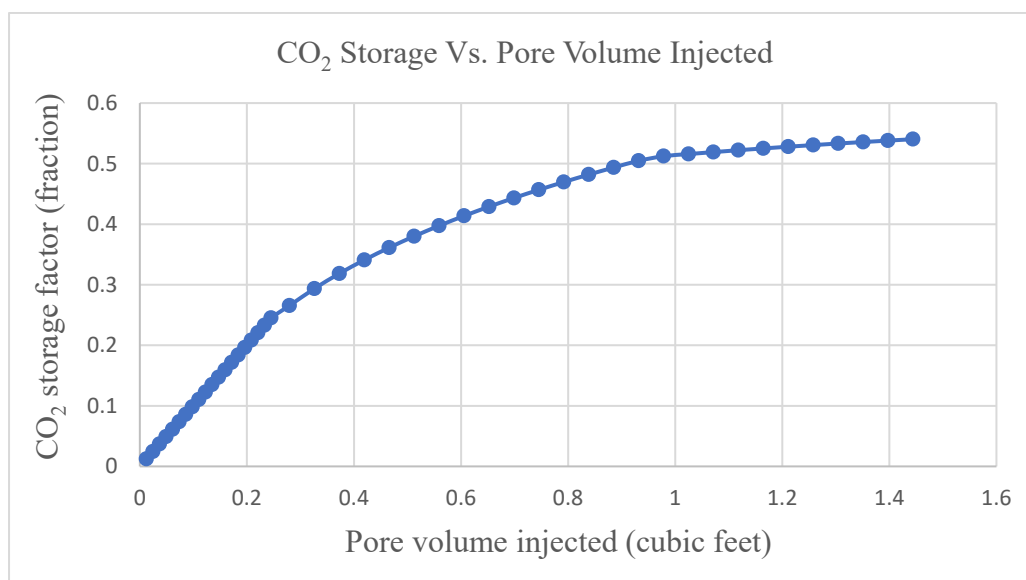


Figure 37: CO₂ storage factor versus pore volume injected for 0.15 cp brine viscosity

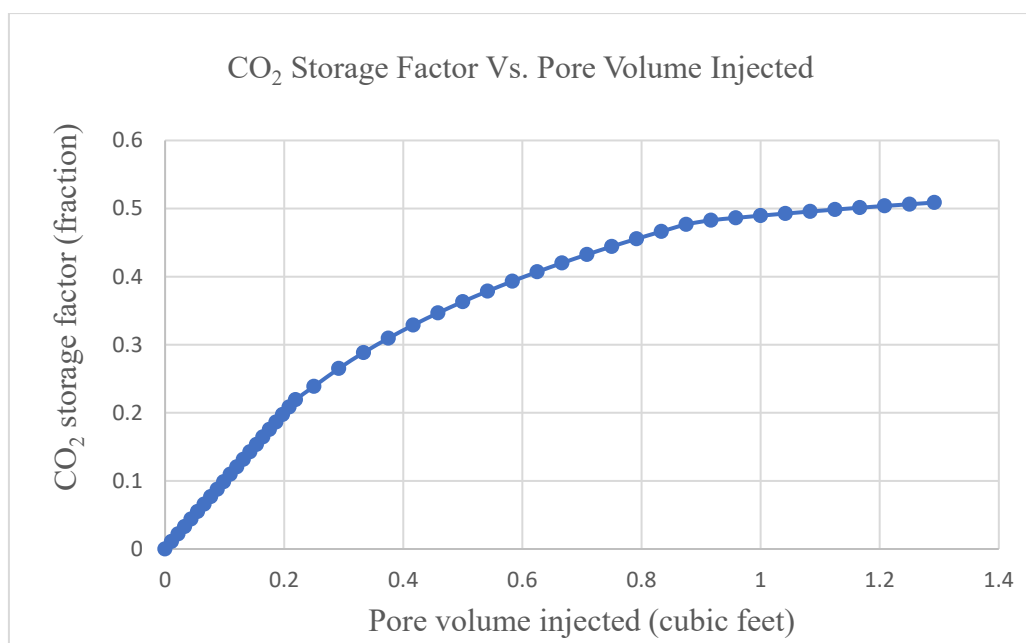


Figure 38: CO₂ storage factor versus pore volume injected for 0.2 cp brine viscosity

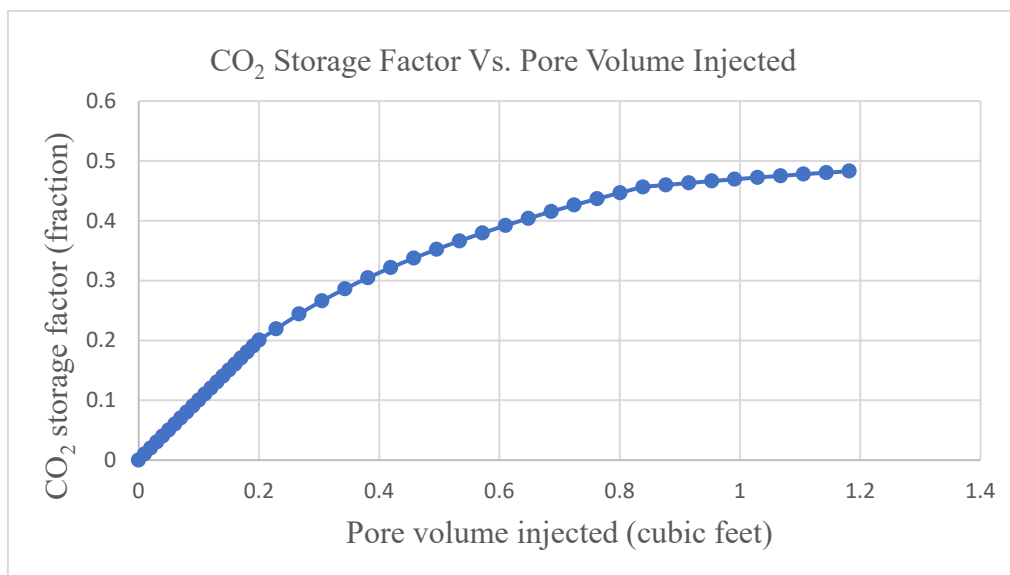


Figure 39: CO₂ storage factor versus pore volume injected for 0.25 cp brine viscosity

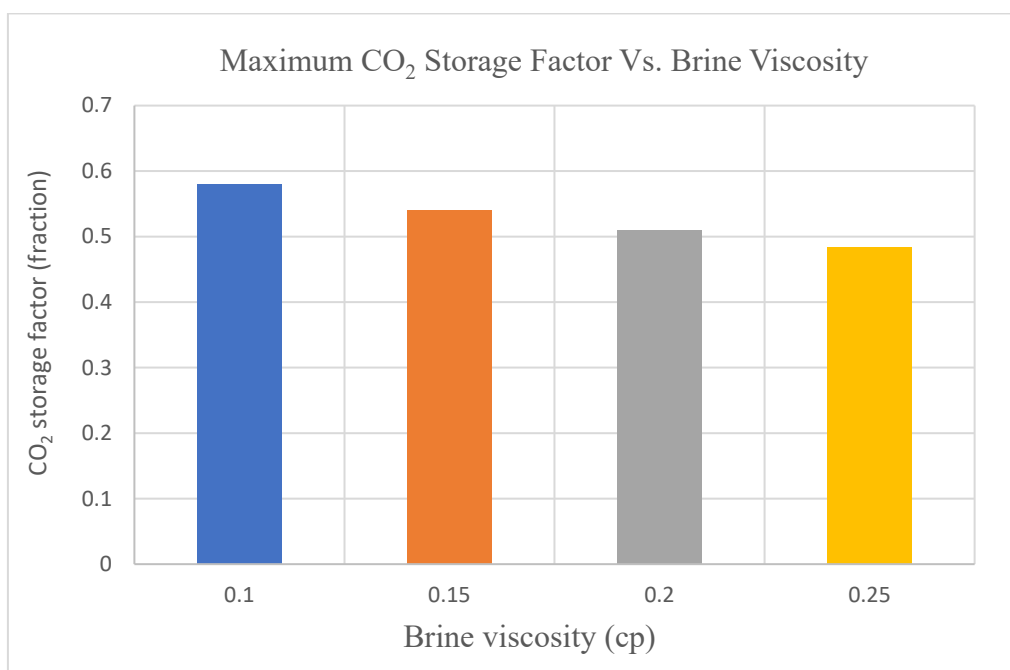


Figure 40: Maximum CO₂ storage factor at each brine viscosity

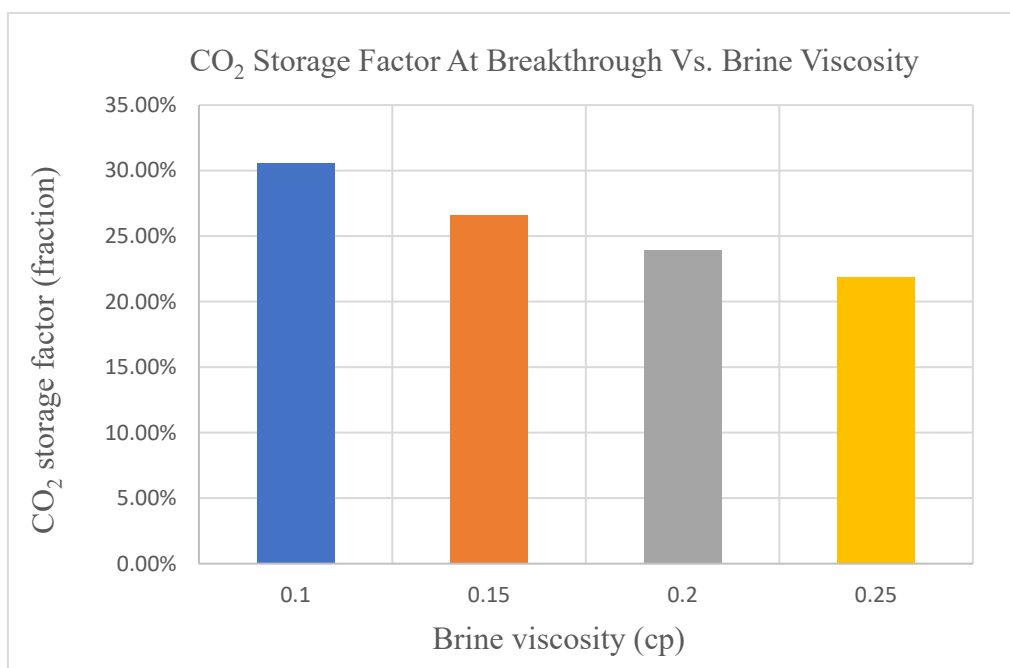


Figure 41: CO₂ storage factor at breakthrough at each brine viscosity

Chapter 5: Discussion

In this section of the report, a detailed discussion will be provided including the capillary pressure curves, pore size distribution, production rates, and the effect of CO₂ storage factor on temperature, gas saturation, and brine viscosity.

5.1 Capillary Pressure and Pore Size Distribution

Figures 10 – 13 show results of the capillary pressure curve for a drainage brine-air process. The capillary pressure relationship is for primary drainage in which the wetting phase (brine) is decreasing from its initial saturation value of 100%. Therefore, the main objective of the capillary pressure curve is to obtain the irreducible water saturation in a rock. This is because it is essential to understand the saturation distribution in the reservoir and the effect of multiphase flow in the rock. Capillary pressure depends on the pore throat size which is related to the grain size and permeability. Rocks have a distribution of pore throat sizes, the bigger the pore size, the lower the capillary pressure (Tiab & Donaldson, 2012).

As shown in Table 6, the irreducible water saturation for each sample was obtained from the capillary pressure curve - drainage process.

Table 6: Irreducible water saturation obtained from porous plate experiment

Core Sample ID	Irreducible water saturation, S_{wirr} (fraction)
9A	0.170
12A	0.180
13A	0.254
14A	0.186

To assess the capillary pressure results obtained through Porous Plate Technique. Pore throat size distribution calculation was conducted using the capillary pressure data for air

displacing water. As mentioned earlier, the objective is to understand the fluid transport in porous media. Table 7 shows the pore throat size distribution that can be achieved at irreducible water saturation. As shown, sample 9A is the lowest since it has the lowest permeability (28 mD) compared to other rock samples. Whereas, core sample 14A shows the maximum pore throat size distribution which has the highest permeability across all samples; 64.08 mD. To support the results of the pore throat size distribution, it is found that as the permeability increases or improved the pore throat size distribution increases. Moreover, any reduction in permeability due to clay swelling, precipitation of organic or inorganic material in porous media can affect the pore size distribution.

Table 7: Pore throat size distribution results

Core Sample ID	Pore throat size distribution @ Swirr (m2)
9A	0.293
12A	0.314
13A	0.408
14A	0.445

5.2 CO₂ Flooding Analysis

The data of core flood experiments are analyzed to determine the endpoints of $K_{r_{CO_2}}$. The relative permeability of carbon dioxide is around 0.85 mD for a reduction in CO₂ saturation from 1.0 to 0.67 on average for all four core samples. The relative permeability of CO₂ increased with the decrease in water saturation. The change in relative permeability of CO₂ endpoints was not relatively significant; a slight change can be seen. Through simulations, the endpoints of $K_{r_{CO_2}}$ for three samples at different temperatures were used to represent the relationship between cumulative time, production rates, CO₂ injection rate, and CO₂ cut. The results of the simulation

run for each sample showed as the temperature increases, a relative increase in brine production rate. Hence, after the CO₂ breakthrough, as the CO₂ cut increases, the brine production drops dramatically and the CO₂ production rate increases with time. CO₂ flooding was conducted at different temperatures and pressure was kept constant. As shown in the flooding test that was conducted at 350, a sharp increase in brine production rate is achieved. The lowest brine recovery was at 200. However, only 50 differences in temperature led which led to a slight increase in brine production rate between 300 and 350. To analyze the performance of brine production rate at a different temperature, the effect of temperature on CO₂ can be explained. typically, both CO₂ solubility in the brine system, as well as the viscosity of brine, have a great impact on the CO₂-Brine system. The solubility of CO₂ in the brine system decreases as the temperature increases. This is mainly related to the brine salinity; as the sodium chloride (NaCl) concentration increases in the brine system, the number of water molecules that will interact with the CO₂ solution will decrease. Therefore, the solubility of CO₂ depends as well on the salinity of the brine; the higher the brine salinity, the lower the CO₂ solubility in brine. Moreover, the temperature has a significant impact on the viscosity of the brine. As the temperature increase, the viscosity of brine decreases. Fluid viscosity is affected by heat, so at high temperatures, the fluid viscosity will decrease. The thermal effect can improve the mobility of the fluid as the viscosity is decreased.

5.3 CO₂ Storage Factor

Based on the results obtained from simulation runs to determine the effect of CO₂ storage on temperature, gas saturation, and brine viscosity conclusions are drawn below.

The first factor that was studied is temperature. As shown from the results, at high temperatures, more CO₂ pore volume is injected so the CO₂ storage factor increases. As shown, as the temperature increases a significant increase in CO₂ storage factor is achieved. Contribution of thermal effects in which CO₂ expands as pressure decreases with depth. Variation in gas saturation had a minor effect on the CO₂ pore volume injected and CO₂ storage factor. Despite the minor change, Figure 34 shows that, as the gas saturation decreases, CO₂ storage capacity increases. The

last factor that was demonstrated is brine viscosity. As shown from the results, as the brine viscosity increases, the CO₂ pore volume injected decreases, and the CO₂ storage factor decreases. Therefore, less volume of CO₂ will be occupied in the reservoir. Also, as shown in Figure 40, the CO₂ storage capacity decreases gradually as the brine viscosity increases.

Chapter 6: Conclusions and Recommendations

6.1 Summary

A supercritical CO₂ flooding experiment was conducted to investigate the effect of temperature change at different brine salinity on the carbon dioxide storage factor. Four selected carbonate – limestone core samples were initially saturated with 100% brine at different brine salinity. The CO₂ core flooding experiments were conducted on the four core samples at constant injection pressure (1270 psi). The temperature of the tested system was varied.

Capillary pressure and relative permeability results were obtained to understand the effect of temperature and brine salinity on the storage capacity of carbon dioxide in a brine aquifer.

6.2 Conclusion

The results of carbon dioxide flooding of a selected aquifer revealed that the CO₂ storage capacity increases as temperature increases due to thermal effects. Whereas, as the gas saturation increases the storage capacity of the selected zone decreases. In addition to that, the flooding runs indicated that relatively high viscosity brine aquifer hider the CO₂ storage capacity of the reservoir.

6.3 Recommendations

Based on the results of the experiment it is recommended to conduct further future work as follows:

1. Investigate the effect of injection pressure on the saline aquifer CO₂ storage capacity.
2. Study the interfacial tension effect between the CO₂ -brine system.
3. Use core samples with wide differences in porosity and permeability to have a better understanding of the flow mechanism.

References

- Abdallah, W., Buckley, J., Carnegie, A., Herold, J., Fordham, E., Graue, A., Signer, T., Hussain, H., Montaron, B. and Ziauddin, M., 2007. Fundamentals of Wettability. [online] Schlumberger Oilfield Review. Retrieved from: <https://www.slb.com/-/media/files/oilfield-review/p44-61-english>. accessed on November, 10, 2022.
- Akbarabadi, M., & Piri, M. (2013). Relative permeability hysteresis and capillary trapping characteristics of supercritical CO₂/brine systems: An experimental study at reservoir conditions. *Advances in Water Resources*, 52, 190-206. <https://doi.org/10.1016/j.advwatres.2012.06.014>.
- Andrei, M., De Simoni, M., Delbianco, A., Cazzani, P., & Zanibelli, L. (2010). *Enhanced Oil Recovery with CO₂ Capture and Sequestration*. Retrieved from: <https://www.osti.gov/etdeweb/biblio/21403705>. accessed on September, 28, 2021.
- Drexler, S., Hoerlle, F., Godoy, W., Boyd, A., & Couto, P. (2020). Wettability alteration by carbonated brine injection and its impact on pore-scale multiphase flow for carbon capture and storage and enhanced oil recovery in a carbonate reservoir. *Applied Sciences*, 10(18), 6496. <https://doi.org/10.3390/app10186496>.
- El-Hoshoudy, A. N., & Desouky, S. (2018). CO₂ miscible flooding for enhanced oil recovery. *Carbon capture, utilization and sequestration*, 79. <https://dx.doi.org/10.5772/intechopen.79082>.
- Glover, P., (2015). Formation Evaluation - Wettability. Retrieved from: Homepages.see.leeds.ac.uk. accessed on November, 05, 2021.
- Honarpour, M. M., Chilingarian, G. V., & Mazzullo, S. J. (1992). Permeability and relative permeability of carbonate reservoirs. In *Developments in petroleum science* (Vol. 30, pp. 399-416). Elsevier. [https://doi.org/10.1016/S0376-7361\(09\)70131-1](https://doi.org/10.1016/S0376-7361(09)70131-1).
- Kim, K., Vilarrasa, V., & Makhnenko, R. Y. (2018). CO₂ Injection Effect on Geomechanical and Flow Properties of Calcite-Rich Reservoirs. *Fluids*, 3(3), 66. <https://doi.org/10.3390/fluids3030066>.
- NETL, (2010). Carbon dioxide enhanced oil recovery-untapped domestic energy supply and long-term carbon storage solution. *The Energy Lab*, Retrieved from: https://www.netl.doe.gov/sites/default/files/netl-file/co2_eor_primer.pdf. accessed on October, 22, 2021.
- PetroWiki. (2015). Miscible flooding - PetroWiki. Copyright 2012-2021. Retrieved from: https://petrowiki.spe.org/Miscible_flooding. accessed on October, 18, 2021.
- Terry, R. and Rogers, J. (2014). Applied petroleum reservoir engineering. 3rd ed, (pp. 357 -368), Upper Saddle River, NJ: Prentice Hall.

- Tiab, D. & Donaldson, E., (2012). *Petrophysics*. 2nd ed, (pp. 342-347). Amsterdam: Gulf Professional Pub.
- Verma, M. K. (2015). *Fundamentals of carbon dioxide-enhanced oil recovery (CO₂-EOR): A supporting document of the assessment methodology for hydrocarbon recovery using CO₂-EOR associated with carbon sequestration* (p. 19). Washington, DC: US Department of the Interior, US Geological Survey.
<https://dx.doi.org/10.3133/ofr20151071>.
- Whittaker, S., & Perkins, E. (2013). Technical aspects of CO₂ enhanced oil recovery and associated carbon storage. *Global CCS institute*, 4-6.

Appendices

Appendix A

- Results of Porous Plate Experiment

Table 8: Capillary pressure results for core sample 9A

Step	Date	Pressure [psig]	Weight after each step [g]	Sw (%)
0		0	139.140	100.0
1	4/12/21	3	136.350	56.6
2	4/25/21	6	135.010	35.8
3	4/29/21	13	134.730	31.4
4	5/10/21	19	134.680	30.6
5	5/23/21	31	134.330	25.2
6	5/27/21	48	134.080	21.3
7	6/3/21	71	133.880	18.2
8	6/9/21	96	133.840	17.6
9	6/16/21	106	133.800	17.0
10				0.0
11				0.0
12				0.0
13				0.0
14				0.0
15				0.0

Table 9: Capillary pressure curve for core sample 12A

Step	Date	Pressure [psig]	Total Weight after each step [g]	Sw (%)
0		0	137.000	100.0
1	4/12/21	3	135.140	63.3
2	4/25/21	6	133.820	37.3
3	4/29/21	13	133.550	32.0
4	5/10/21	19	133.330	27.6
5	5/23/21	31	133.170	24.5
6	5/27/21	48	132.990	20.9
7	6/3/21	71	132.890	18.9
8	6/9/21	96	132.860	18.3
9	6/16/21	106	132.840	17.9
10				0.0
11				0.0
12				0.0
13				0.0
14				0.0
15				0.0

Table 10: Capillary pressure curve for core sample 13A

Step	Date	Pressure [psig]	Total Weight after each step [g]	Sw (%)
0		0	139.770	100.0
1	4/12/21	3	139.390	89.9
2	4/25/21	6	137.900	50.5
3	4/29/21	13	137.630	43.4
4	5/10/21	19	137.470	39.2
5	5/23/21	31	137.260	33.6
6	5/27/21	48	137.110	29.6
7	6/3/21	71	136.960	25.7
8	6/9/21	96	136.970	25.9
9	6/16/21	106	136.950	25.4
10				0.0
11				0.0
12				0.0
13				0.0
14				0.0
15				0.0

Table 11: Capillary pressure curve for core sample 12A

Step	Date	Pressure [psig]	Total Weight after each step [g]	Sw (%)
0		0	135.370	1
1	4/12/21	3	134.710	0.867735471
2	4/25/21	6	132.810	0.486973948
3	4/29/21	13	132.320	0.388777555
4	5/10/21	19	131.990	0.322645291
5	5/23/21	31	131.760	0.276553106
6	5/27/21	48	131.560	0.236472946
7	6/3/21	71	131.350	0.194388778
8	6/9/21	96	131.330	0.190380762
9	6/16/21	106	131.310	0.186372745
10				0
11				0
12				0
13				0
14				0
15				0

Appendix B

- Pore throat size distribution results

Table 12: Pore throat size distribution results for core sample 9A

PV (cm3)	6303.922			
(dS/dP) psia	Pressure (psia)	Ri (microns)	D(ri), cm2	D(ri), m2
14.53929497	17.4	8.275862069	418360.3378	0.041836034
14.63144798	20.4	7.045009785	494568.1087	0.049456811
14.69384075	27.51	5.234460196	668472.9351	0.066847294
14.69875184	33.7	4.267931239	820131.41	0.082013141
14.6954488	45.7	3.150984683	1110598.195	0.111059819
14.69771293	62.7	2.296650718	1523965.764	0.152396576
14.69864764	85.7	1.680280047	2083128.738	0.208312874
14.69975117	110.7	1.300813008	2691011.249	0.269101125
14.69937792	120.7	1.193040597	2934027.195	0.293402719

Table 13: Pore throat size distribution results for core sample 12A

PV (cm3)	3375			
(dS/dP) psia	Pressure (psia)	Ri (microns)	D(ri), cm2	D(ri), m2
14.56412448	17.4	8.275862069	448847.132	0.044884713
14.6143569	20.4	7.045009785	529084.9701	0.052908497
14.69246755	27.5	5.234460196	715896.3606	0.071589636
14.69303491	33.7	4.267931239	878054.3783	0.087805438
14.69736136	45.7	3.150984683	1189653.252	0.118965325
14.69791159	62.7	2.296650718	1632254.955	0.163225495
14.69914244	85.7	1.680280047	2231195.598	0.22311956
14.69976331	110.7	1.300813008	2882191.194	0.288219119
14.69960552	120.7	1.193040597	3142518.003	0.3142518

Table 14: Pore throat size distribution results for core sample 13A

PV (cm3)	4377.192982			
(dS/dP) psia	Pressure (psia)	Ri (microns)	D(ri), cm2	D(ri), m2
14.662767	17.4	8.275862069	586381.0124	0.058638101
14.57033556	20.4	7.045009785	684486.9343	0.068448693
14.68989695	27.5	5.234460196	928803.9568	0.092880396
14.69320577	33.7	4.267931239	1139400.37	0.113940037
14.69535489	45.7	3.150984683	1543515.503	0.15435155
14.69766573	62.7	2.296650718	2118022.767	0.211802277
14.69827467	85.7	1.680280047	2895088.86	0.289508886
14.70010582	110.7	1.300813008	3740096.426	0.374009643
14.6994709	120.7	1.193040597	4077779.049	0.407777905

Table 15: Pore throat size distribution results for core sample 14A

PV (cm3)	4783.018868			
(dS/dP) psia	Pressure (psia)	Ri (microns)	D(ri), cm2	D(ri), m2
14.65101314	17.4	8.275862069	640232.9522	0.064023295
14.5747495	20.4	7.045009785	748174.8542	0.074817485
14.68611084	27.5	5.234460196	1014655.255	0.101465525
14.68938487	33.7	4.267931239	1244714.661	0.124471466
14.69614614	45.7	3.150984683	1686711.396	0.16867114
14.69764234	62.7	2.296650718	2314388.874	0.231438887
14.69817025	85.7	1.680280047	3163480.871	0.316348087
14.69983968	110.7	1.300813008	4086780.723	0.408678072
14.6995992	120.7	1.193040597	4455884.043	0.445588404

Appendix C

- Experimental CO₂ Flooding Test

Table 16: CO₂ flooding test for sample 9A

CO₂ flooding conditions						
Temperature (F):	150					
Over burden pressure (psi):	2500					
Injecting pressure (psi):	1270					
Back Pressure (psi):	1200					
CO₂ flooding test						
Tube no.	Time (sec)	Water volume (cc)	Water in place (cc)	Sw (%)	Sco ₂ (%)	Sco ₂
1	60	0.9	5.40	85.7	14.3	0.143
2	60	1	4.40	69.9	30.1	0.301
3	60	0.8	3.60	57.2	42.8	0.428
4	60	0.7	2.90	46.1	53.9	0.539
5	60	0.9	2.00	31.8	68.2	0.682
6	60	0.6	1.40	22.3	77.7	0.777
7	60	0.2	1.20	19.1	80.9	0.809
8	60	0.05	1.15	18.3	81.7	0.817
9	60	0.01	1.14	18.1	81.9	0.819
10	600	0.001	1.14	18.1	81.9	0.819

Table 17: CO₂ flooding test for sample 12A

CO₂ flooding conditions						
Temperature (F):	200					
Over burden pressure (psi):	2500					
Injecting pressure (psi):	1270					
Back Pressure (psi):	1200					
CO₂ flooding test						
Tube no.	Time (sec)	Water volume (cc)	Water in place (cc)	Sw (%)	Sc _{o2} (%)	Sc _{o2}
1	60	1	3.78	79.1	20.9	0.209
2	60	0.9	2.88	60.3	39.7	0.397
3	60	0.9	1.98	41.5	58.5	0.585
4	60	0.2	1.78	37.3	62.7	0.627
5	600	0.2	1.58	33.1	66.9	0.669
6	600	0.01	1.57	32.9	67.1	0.671
7	600	0.01	1.56	32.7	67.3	0.673
8	600	0.01	1.55	32.5	67.5	0.675
9	600	0.01	1.54	32.3	67.7	0.677
10	1200	0.01	1.53	32.1	67.9	0.679

Table 18: CO₂ flooding test for sample 13A

CO₂ flooding conditions						
Temperature (F):	250					
Over burden pressure (psi):	2500					
Injecting pressure (psi):	1270					
Back Pressure (psi):	1200					
CO₂ flooding test						
Tube no.	Time (sec)	Water volume (cc)	Water in place (cc)	Sw (%)	Sc _{o2} (%)	Sc _{o2}
1	60	0.9	2.48	73.3	26.7	0.3
2	60	0.9	1.58	46.7	53.3	0.5
3	60	0.6	0.98	28.9	71.1	0.7
4	60	0.01	0.97	28.6	71.4	0.7
5	600	0.01	0.96	28.3	71.7	0.7
6	600	0.01	0.95	28.0	72.0	0.7
7	600	0.01	0.94	27.7	72.3	0.7
8	600	0.001	0.93	27.7	72.3	0.7

Table 19: CO₂ flooding test for sample 14A

CO₂ flooding conditions						
Temperature (F):	300					
Over burden pressure (psi):	2500					
Injecting pressure (psi):	1270					
Back Pressure (psi):	1240					
CO₂ flooding test						
Tube no.	Time (sec)	Water volume (cc)	Water in place (cc)	Sw (%)	Sc _{o2} (%)	Sc _{o2}
1	60	0.9	7.54	89.3	10.7	0.107
2	60	1	6.54	77.5	22.5	0.225
3	60	0.9	5.64	66.8	33.2	0.332
4	60	0.9	4.74	56.2	43.8	0.438
5	60	1	3.74	44.3	55.7	0.557
6	60	0.6	3.14	37.2	62.8	0.628
7	60	0.2	2.94	34.8	65.2	0.652
8	600	0.1	2.84	33.6	66.4	0.664
9	600	0.1	2.74	32.5	67.5	0.675
10	600	0.1	2.64	31.3	68.7	0.687
11	600	0.1	2.54	30.1	69.9	0.699
12	600	0.1	2.44	28.9	71.1	0.711
13	600	0.1	2.34	27.7	72.3	0.723
14	600	0.1	2.24	26.5	73.5	0.735
15	600	0.001	2.24	26.5	73.5	0.735

The logo of the United Arab Emirates University (UAEU) is displayed in a red rectangular box. It consists of the letters 'UAEU' in a white, bold, sans-serif font.

جامعة الإمارات العربية المتحدة
United Arab Emirates University



UAE UNIVERSITY MASTER THESIS NO. 2022:11

The objective of this paper is to perform laboratory measurements and CO₂ underground storage study. The results of both CO₂-brine flooding experiment and simulations that were conducted to understand the effect of brine viscosity, temperature, gas saturation. The results showed that CO₂ storage capacity increases as temperature increases. Yet, the presence of free gas has a negative effect on storage factor. Moreover, the CO₂ storage factor decreases gradually as the brine viscosity increases.

Sarah Al-Tamimi received her Master of Science in Petroleum Engineering from the Department of Chemical and Petroleum Engineering, College of Engineering at UAE University, UAE. She received her BSc from the College of Petroleum Engineering, Khalifa University, Abu Dhabi.

www.uaeu.ac.ae